

# MTG1 couples mitoribosome large subunit assembly with intersubunit bridge formation

Hyun-Jung Kim<sup>1</sup> and Antoni Barrientos<sup>1,2,\*</sup>

<sup>1</sup>Department of Biochemistry and Molecular Biology, University of Miami Miller School of Medicine, Miami, FL 33136, USA and <sup>2</sup>Department of Neurology, University of Miami Miller School of Medicine, Miami, FL 33136, USA

Received May 15, 2018; Revised July 11, 2018; Editorial Decision July 12, 2018; Accepted July 13, 2018

## ABSTRACT

**Mammalian mitochondrial ribosomes (mitoribosomes) synthesize 13 proteins, essential components of the oxidative phosphorylation system. They are linked to mitochondrial disorders, often involving cardiomyopathy. Mitoribosome biogenesis is assisted by multiple cofactors whose specific functions remain largely uncharacterized. Here, we examined the role of human MTG1, a conserved ribosome assembly guanosine triphosphatase. *MTG1*-silencing in human cardiomyocytes and developing zebrafish revealed early cardiovascular lesions. A combination of gene-editing and biochemical approaches using HEK293T cells demonstrated that MTG1 binds to the large subunit (mtLSU) 16S ribosomal RNA to facilitate incorporation of late-assembly proteins. Furthermore, MTG1 interacts with mtLSU uL19 protein and mtSSU mS27, a putative guanosine triphosphate-exchange factor (GEF), to enable MTG1 release and the formation of the mB6 intersubunit bridge. In this way, MTG1 establishes a quality control checkpoint in mitoribosome assembly. In conclusion, MTG1 controls mitochondrial translation by coupling mtLSU assembly with intersubunit bridge formation using the intrinsic GEF activity acquired by the mtSSU through mS27, a unique occurrence in translational systems.**

## INTRODUCTION

Mitochondria are eukaryotic organelles derived from early endosymbiotic bacteria capable of oxidative phosphorylation (OXPHOS) (1). Present-day mitochondria have retained their own genome (mitochondrial DNA, mtDNA), which in mammals encodes 13 proteins, all of which are essential components of the OXPHOS enzymatic complexes.

These proteins, largely hydrophobic, are synthesized in specialized mitochondrial ribosomes of bacterial descent (mitoribosomes) located in the matrix and tethered to the inner membrane to facilitate co-translational insertion of newly synthesized proteins. The complete mammalian mitoribosome is a 55S RNA–protein complex consisting of a large subunit (mtLSU, 39S) and a small subunit (mtSSU, 28S). These subunits contain the mtDNA-encoded 16S ribosomal RNA (rRNA) and 12S rRNA, respectively, and more than 80 mitoribosome proteins (MRPs) encoded in the nuclear DNA (nDNA) (2,3). Recent data have shown that the human mtLSU also contains a structural tRNA<sup>Val</sup>, which replaces bacterial and eukaryotic 5S rRNA (2,3). Mitoribosomes are biomedically relevant because they share sensitivity to antibiotics similar to common infectious bacteria. Also, they are emerging as new targets for cancer therapeutics (4). At last, mutations in MRPs, rRNAs and translation factors are responsible for a heterogeneous group of human multisystemic OXPHOS disorders, frequently involving sensorineural hearing loss, encephalomyopathy and hypertrophic cardiomyopathy (5).

For all ribosomes, biogenesis of each subunit proceeds via independent pathways (6–9). Ribosome subunit assembly involves the coordinated processing and modification of rRNAs with the association of ribosomal proteins. The assembly process is assisted by several classes of cofactors, including guanosine triphosphatases (GTPases), DEAD-box RNA helicases, kinases, RNA modification enzymes and chaperone proteins (5,10). For the mitoribosome, initial assembly landscapes for yeast and human subunits have been only recently reported (6,9), and the identity and function of assembly factors (AFs) are merely starting to emerge (11–15). Given the rRNA conformational changes that occur during ribosome assembly and the necessity to resolve possible kinetic traps, the requirement for nucleoside triphosphates (NTP) hydrolyzing enzymes is not surprising (16). Focusing on GTPases, a subset of these regulatory proteins is involved in ribosome subunit assembly. In bacteria, with seven members involved, GTPases represent the largest class of essential ribosome AFs (10,17). In human

\*To whom correspondence should be addressed. Tel: +305 243 8683; Fax: +305 243 7404; Email: abarrientos@med.miami.edu

mitochondria, two conserved GTPases are known to be involved in mtSSU biogenesis: C4orf14 (bacterial YqeH) (18) and ERAL1 (bacterial Era1) (19). Two other GTPases are required for mtLSU assembly: OBGH1 (bacterial ObgE) and MTG1 (bacterial RbgA) (20). However, their molecular functions remain unknown.

As a case in point, whereas bacterial RbgA/YlqF is extensively characterized structurally and functionally, little is known regarding its mitochondrial MTG1 counterpart, particularly in human cells. All members of the RbgA/YlqF GTPase subfamily, which contains a unique circular permutation of the guanosine triphosphate (GTP)-binding domain (cpGTPase), interact with RNA and are involved in ribosome assembly (10). Absent in *Escherichia coli*, the most studied *Bacillus subtilis* RbgA participates in the late steps of 50S ribosomal LSU assembly and maturation (21). It interacts with the 50S (to specific positions in 23S rRNA) in a GTP-dependent manner, and its GTPase activity is stimulated more than 60-fold by the association with the 50S subunit *in vitro* (22–24). After GTP hydrolysis, RbgA dissociates from the ribosome (25). RbgA-depleted cells do not form mature 50S but instead accumulate a 45S intermediate complex that contains substoichiometric amounts of late-assembly LSU proteins: L16, L27, L28, L33, L35 and L36 (23,25–29). The *rbgA* LSU assembly defect is attenuated by mutations in L6, which has suggested that RbgA could facilitate proper incorporation of L6 to the LSU assembly line, subsequently triggering the integration of late-assembly proteins (26). In mitochondria, MTG1 was first identified in the yeast *Saccharomyces cerevisiae* as required for mtLSU 21S rRNA stability and mitochondrial protein synthesis (30). This phenotype is partially suppressed by spontaneous mutations in the 21S rRNA domain V, strongly suggesting a direct role of yeast MTG1 in mtLSU biogenesis. As in yeast, human MTG1 is known to localize to mitochondria, and *MTG1* silencing in HeLa cells partially attenuates mitochondrial translation (20). The intrinsic recombinant MTG1 GTPase activity is undetectable, but it is stimulated *in vitro* by the mtLSU (20). Importantly, heterologous expression of human *MTG1* partially rescues the mitochondrial protein synthesis defect in yeast *mtg1* null mutant cells (30). These observations suggest that human MTG1 could also participate in mtLSU assembly although its precise molecular role remains unknown.

In this study, we have used gene editing and RNA interference (RNAi) approaches to generate MTG1-depleted cell lines and organisms, which we have characterized molecularly, biochemically and physiologically. *MTG1*-silencing in human cardiomyocytes and developing zebrafish revealed early cardiovascular lesions. Mechanistically, data obtained using *MTG1*-KO HEK293T cells in parallel with *in vitro* assays provide unrecognized insights into the role of human MTG1 in mtLSU assembly. They also reveal that the release of MTG1 from the mtLSU is triggered by subunit joining during monosome formation, with one of the mtSSU subunits acting as a guanosine diphosphate (GDP) exchange factor. In this way, MTG1 sets a quality control checkpoint in mitoribosome assembly that controls mitochondrial translation, by coupling mitoribosome LSU assembly with intersubunit bridge formation.

## MATERIALS AND METHODS

### Human cell lines and culture conditions

HEK293T embryonic kidney cells (CRL-3216) and 143B osteosarcoma cells (CRL-8303) were obtained from ATCC. The 143B.TK<sup>-</sup> rho<sup>0</sup> derivative (143B206) was obtained from Dr M. King (31). The three cell lines were cultured at 37°C under 5% CO<sub>2</sub> in high-glucose Dulbecco's Modified Eagle's Medium (DMEM) medium supplemented with 10% fetal bovine serum (FBS), 1 mM pyruvate and 50 µg/ml uridine (complete DMEM medium). Analysis for mycoplasma contamination was routinely performed.

iCell cardiomyocytes derived from induced pluripotent stem (iPS) cells were obtained from Cellular Dynamics (Madison, WI). These human heart cells consist of a 95% pure population of ventricular, atrial and nodal cells. They are known to recapitulate healthy human cardiac biology. Plating and maintenance media were obtained from Cellular Dynamics (<https://cellulardynamics.com/products-services/icell-products/icell-cardiomyocytes/>). Assays in cardiomyocytes are described in the Supplementary Data.

### Key reagents

Tables presenting the list of antibodies, recombinant DNAs, oligonucleotides and Small interfering RNA (siRNA) oligonucleotides used in this study are included in the Supplementary Data.

### Generation of *MTG1*-KO cell lines

To create a stable human *MTG1* knockout (KO) line in HEK293T cells, we used transcription activator-like effector nuclease (TALEN) constructs obtained from Collectis (Paris, France). Two pairs of TALENs (32 and #2) were designed. The left and right TALENs for each pair were designed to bind the sequences shown in Figure 2A. Details on plasmid transfection, *MTG1*-KO clone selection and genotyping are presented in the Supplementary Data.

To establish stable lines expressing tagged or untagged versions of MTG1 or other genes of interest, 4 µg of pIRE-Spuro2 empty vector or pIRESpuro2 containing FLAG-tagged *MTG1* was transfected to HEK293T cells using a standard Lipofectamine 2000 protocol. Two days after transfection, the medium was supplemented with 2.5 µg/ml puromycin for 3 weeks.

### Pulse labeling of mitochondrial translation products

Mitochondrial protein synthesis was assayed by pulse-labeling 80% confluent human HEK293T and cardiomyocyte cultures in the presence of 100 µl/ml emetine to inhibit cytoplasmic protein synthesis as reported (33,34) and described in 'Supplementary Materials and Methods' section.

### Isolation of mitochondria

Mitochondria from wild-type (WT) HEK293T cells or HEK293T cells stably expressing MTG1-FLAG were isolated as described previously (35).

### Sucrose gradient analysis

The sedimentation properties of MTG1 and mitoribosomal proteins were analyzed by sucrose gradient sedimentation essentially as reported (15) and described in ‘Supplementary Materials and Methods’ section.

### RNA analysis

Total RNA was prepared from whole cells by using Trizol (Invitrogen) following the manufacturer instructions for northern blot and quantitative polymerase chain reaction (qPCR) analyses. Experimental details are described in ‘Supplementary Materials and Methods’ section.

### MTG1 interactome analysis

To study the MTG1 protein interactome, we used modified versions of co-immunoprecipitation analysis of protein–protein interaction in the presence or absence of cross-linkers. We also used modified versions of PAR-CLIP assays to study protein–RNA interactions (36). Experimental details are described in ‘Supplementary Materials and Methods’ section.

### Zebrafish husbandry

Zebrafish were freshly supplied from University of Miami Zebrafish Core Facility and maintained in the facility during analysis. Experiments were carried out using *Danio rerio* WT strains AB. Embryos were obtained from natural crosses after removing a divider at first light and microinjections were performed into one-cell stage embryos. Embryos were reared in Petri dishes of system water in a 28°C incubator with a 14-h light/10-h dark cycle. All experiments were conducted in accordance with the University of Miami Institutional Animal Care and Use Committee guidelines. Assays in zebrafish are described in the Supplementary Data.

### Statistical analysis

All of the experiments were done at least in triplicate or otherwise indicated. Data in X-ray films were digitalized and analyzed using the ImageJ software. Statistical analyses were performed using the Prism-6 software. The data are presented as the means  $\pm$  S.D. of absolute values or percentages of control. The values obtained for WT, a *MTG1* partial KO (*MTG1*-KO 1F5), and the clone after silencing of *MTG1* (*MTG1*-KO 1F5-si*MTG1*) strains for the different parameters studied were compared using a Student’s two-tailed *t*-test for comparison of two groups. For comparison of multiple groups, we performed one-way analysis of variance (ANOVA) followed by Tukey’s *post hoc* test for all groups of the experiment. The statistical significance of cardiomyocyte and zebrafish studies were tested with one-way ANOVA followed by a Sidak’s or a Tukey’s multiple comparison test, respectively. The statistical tests of *MTG1*–rRNAs interaction were analyzed with two-way ANOVA followed by a Tukey’s *post hoc* test (\* $P < 0.05$ ; \*\* $P < 0.01$ ; \*\*\* $P < 0.001$ ; \*\*\*\* $P < 0.0001$ ).

## RESULTS AND DISCUSSION

### MTG1 is a mitochondrial peripheral inner membrane protein that interacts with the mtLSU

Human MTG1 was previously localized to mitochondria in HeLa cells (20). To confirm and expand these observations, we used HEK293T cells to pursue several approaches. Cell fractionation experiments to isolate mitochondria followed by brief sonication to separate soluble and insoluble fractions, alkaline carbonate extraction to separate membrane intrinsic and extrinsic proteins, and proteinase protection assays to determine MTG1 submitochondrial localization and topology (Supplementary Figure S1A and B) in conjunction with fluorescence immunohistochemistry (Supplementary Figure S1C) allowed us to confirm that MTG1 is a mitochondrial protein. The data obtained (Supplementary Figure S1A and B) also lead us to conclude that MTG1 is a matrix protein loosely associated with the inner membrane, the location and behavior expected of a ribosome assembly protein.

To test whether the steady-state levels of MTG1 depend on the presence of mitochondrial ribosomes, we estimated MTG1 steady-state levels in a derivative of an osteosarcoma 143B cell line devoid of mtDNA ( $\rho^{\circ}$  cells) and therefore of all mitochondrial RNA (mtRNAs) including rRNAs. Several ribosome proteins tested (uL16, uL19 and bS18) did not accumulate in  $\rho^{\circ}$  cells and other (mS27) were markedly decreased (Figure 1A), whereas only traces of MTG1 were detected. These data could link MTG1 to mitoribosome biogenesis, similar to all its homologs, but in principle, also to mtDNA or mtRNA transactions.

To explore a possible association of MTG1 with the mitoribosome, we used sucrose gradient sedimentation analysis of mitochondrial extracts prepared in the presence of 5 mM ethylenediaminetetraacetic acid (EDTA) to favor dissociation into ribosome subunits (Figure 1B). In 143B-WT cells, a portion of MTG1 (~10% of total) co-sediments with mtLSU markers, whereas the rest accumulates in lighter fractions in which a calibration marker (lactate dehydrogenase (LDH), 130 kDa) peaks. In 143B- $\rho^{\circ}$  cells, the ribosome subunits are obviously not formed, and the residual MTG1 only forms slow sedimenting particles (Figure 1B). Studies in HEK293T mitochondrial extracts consistently identified a portion of MTG1 molecules co-sedimenting with the mtLSU, when they were prepared either in the presence of EDTA (Figure 1C) or in the presence of 10 mM  $Mg^{2+}$  to favor the stability of the monosome (Figure 1D). Further exploration of MTG1 sedimentation patterns in gradients prepared using whole HEK293T cell extracts allowed us to identify a small portion of MTG1 that additionally co-sediments with the 55S monosome (Figure 1E). This interaction must be very transient or labile since it is not detectable following the mechanical stress the cells undergo during mitochondrial isolation. Therefore, MTG1 may play a role in mtLSU biogenesis that extends until the formation of the monosome.

### MTG1 is required for HEK293T cell proliferation

To gain insight into the specific role of MTG1 in mitochondrial translation and mitoribosome assembly, we at-

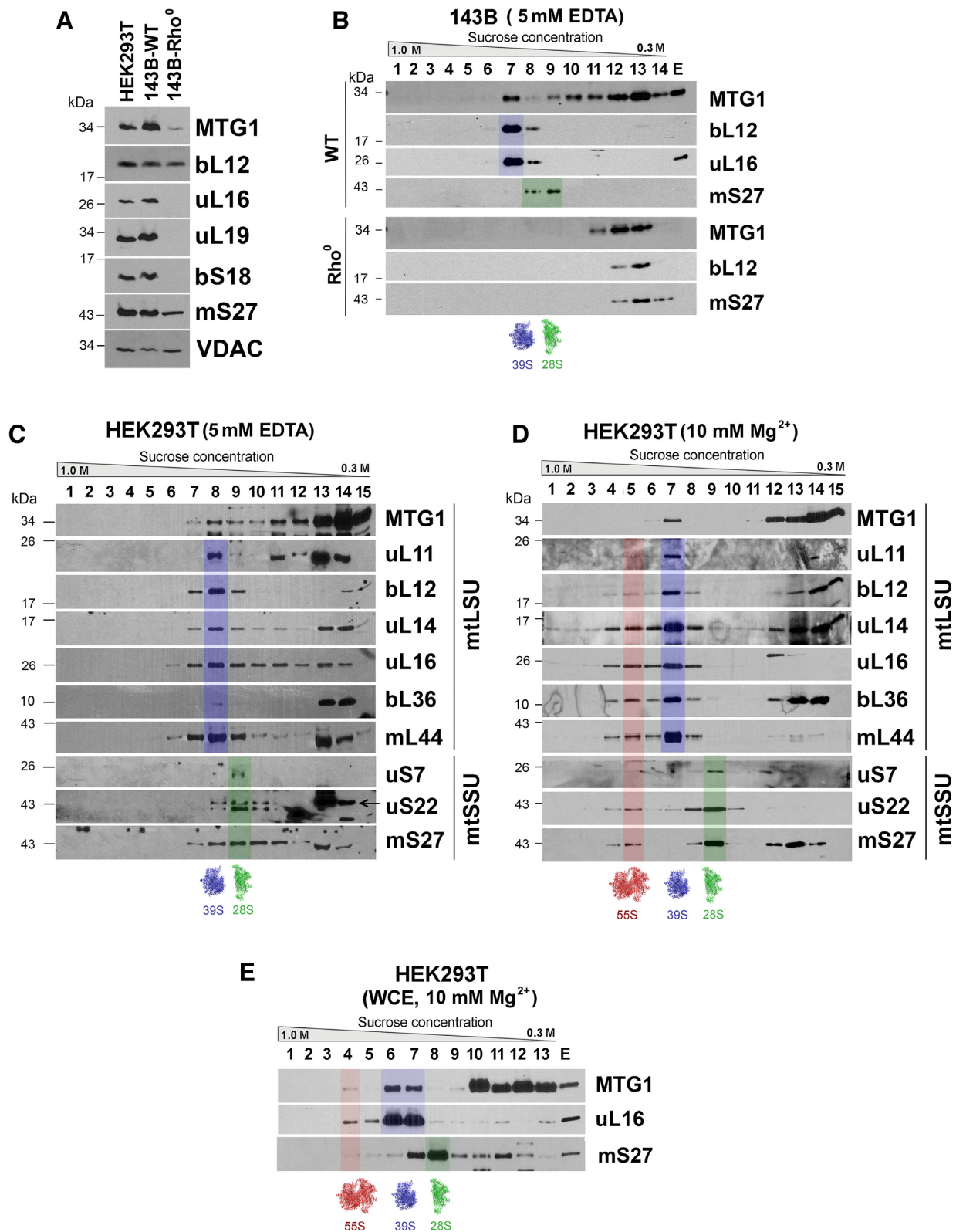


**Figure 1.** MTG1 is a mitochondrial protein that interacts with the mitoribosome large subunit (mtLSU). (A) Immunoblot analyses of the steady-state levels of MTG1 and indicated mtLSU and mtSSU proteins in HEK293T, 143B and 143B-206 rho<sup>o</sup> cells. voltage-dependent anion channel (VDAC) was used as loading control. (B) Sucrose gradient sedimentation analyses of mtSSU (mS27) and mtLSU proteins (bL12 and uL16) in mitochondrial extracts from 143B WT and 206 rho<sup>o</sup> cells, prepared in the presence of 5 mM EDTA. (C and D) Sucrose gradient sedimentation analyses of MTG1 and indicated MRPs in mitochondrial extracts from HEK293T cells, prepared in the presence of either (C) 5 mM EDTA or (D) 10 mM MgCl<sub>2</sub>. (E) Sucrose gradient sedimentation analyses of MTG1 and indicated MRPs in whole-cell extracts (WCE) from HEK293T cells, prepared in the presence of 10 mM MgCl<sub>2</sub>. Transparent red, purple and green colors mark the fractions where the 55S monosome, 39S mtLSU and 28S mtSSU sediment, respectively.

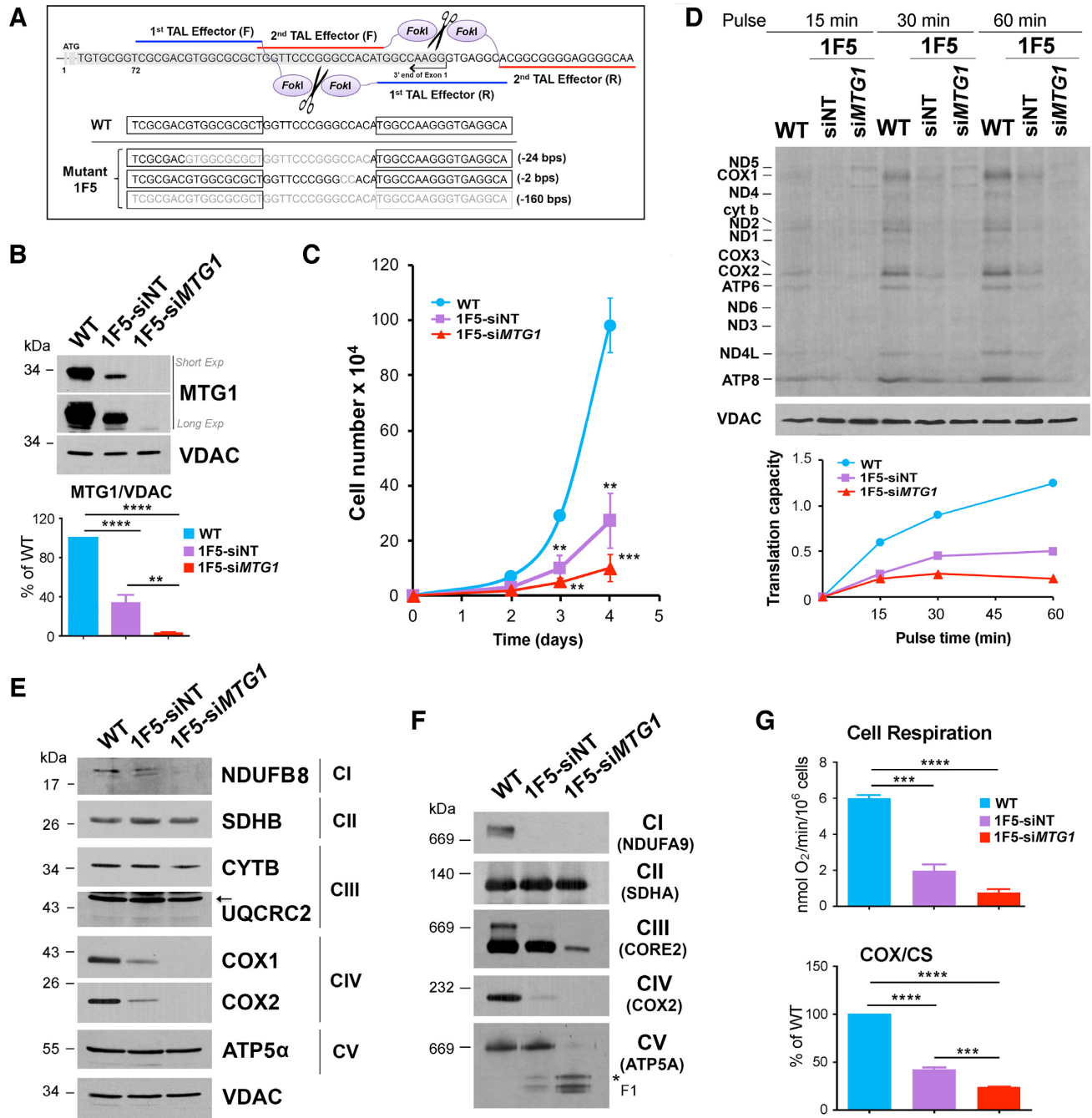


**Figure 2.** MTG1 is required for efficient mitochondrial translation and OXPHOS function in HEK293T cells. (A) Schematics of the first exon of the *MTG1* locus and the sequences recognition sites of two different TALEN pairs. The genotyping of a three-allele compound heterozygous *MTG1*-KO clone, 1F5, is depicted. (B) Immunoblot analysis of the steady-state levels of MTG1 in HEK293T (WT), *MTG1*-KO clone 1F5 and the 1F5 clone treated for 5 days with siMTG1. VDAC was used as a loading control. Two exposures of the anti-MTG1 immunoblot (short and long) are presented. The lower panel shows the densitometry values normalized by the signal of VDAC and expressed relative to the WT; one-way ANOVA with a Tukey's multiple comparisons test: \*\**P* < 0.01; \*\*\*\**P* < 0.0001. (C) Cell proliferation assay of the WT, *MTG1*-KO clone 1F5 and the 1F5 clone treated for 5 days with siMTG1; one-way ANOVA with a Tukey's multiple comparisons test: \*\**P* < 0.01; \*\*\**P* < 0.001. (D) Metabolic labeling with <sup>35</sup>S-methionine of newly synthesized mitochondrial translation products in whole cells from the indicated lines during increasing pulse times in the presence of emetine to inhibit cytoplasmic protein synthesis. Immunoblotting for VDAC was used as a loading control. Newly synthesized polypeptides are identified on the right. The lower panel shows the densitometry values (average of ND2, COX2 and ATP8 signals) normalized by the signal of VDAC and expressed relative to the WT. (E) Immunoblot analysis of OXPHOS complex subunits in the indicated cell lines. NDUFB8 is a subunit of complex I, SDHB of CII, UQCRC2 or CIII, COX1 and COX2 of CIV, ATP5 $\alpha$  of the F<sub>1</sub>F<sub>0</sub>-ATP synthase or CV. Immunoblotting for VDAC was used as a loading control. (F) Steady-state levels of OXPHOS complexes extracted with lauryl maltoside in the indicated cell lines, analyzed by BN-PAGE and detected by immunoblotting with the indicated antibodies. (G) Measurement of OXPHOS parameters in the indicated cell lines. The upper graph shows the endogenous cell respiration rate. The lower graph shows the enzymatic activity of CIV or cytochrome *c* oxidase (COX) normalized by the activity of citrate synthase (CS) and expressed as percentage of WT. In all graphs, data represent the mean  $\pm$  SD of three independent repetitions; one-way ANOVA with a Tukey's multiple comparisons test: \*\*\**P* < 0.001; \*\*\*\**P* < 0.0001.

tempted to engineer KO of *MTG1* in HEK293T cells using a TALEN-mediated approach. Although several transfection strategies and TALEN pairs were used and nearly 1000 clones were analyzed, we did not identify any homozygous KO. Consistently, *MTG1* could not be KO in either haploid HAP1 cells (Horizon Discovery, UK; not shown), which suggested possible essentiality for this gene. However, among the many heterozygous HEK293T clones obtained, as screened by immunoblot against MTG1, one clone obtained with the first-TALEN-pair (Figure 2A) had detectable but particularly low residual MTG1 levels (Figure 2B). By genotyping, the clone (*MTG1*-KO 1F5) was found to harbor two null *MTG1* alleles, and a third allele carrying an in-frame 24-nt deletion within the TALEN spacer region (Figure 2A). *MTG1*-KO 1F5 has a proliferation rate in standard high-glucose DMEM media considerably slower than WT cells (Figure 2C). To test whether the residual protein was still functional, the clone was subsequently treated with double strand siRNA for *MTG1* gene-silencing. After 5 days of siRNA transfection, steady-state levels of MTG1 were undetectable (Figure 2B), what further decreased the ability of the cells to proliferate (Figure 2C), indicating that the truncated MTG1 protein is functional.

Attempts to use the *MTG1*-KO 1F5 clone to generate homozygous KO clones by using additional TALEN constructs (second TALEN pairs in Figure 2A) were not successful. However, the *MTG1*-KO 1F5 clone is still a very useful resource, because siRNA-mediated silencing of *MTG1* is markedly more effective in this cell line than that in WT HEK293T cells (Supplementary Figure S2A).

The apparent essentiality of *MTG1* was also manifested when performing siRNA-mediated silencing of its expression, a manipulation that induced severe cell death if extended for more than 5 days. Therefore, we used this time frame in all our silencing experiments. In regular *MTG1*-KO 1F5 cultures but not in WT cell cultures, abundant floating cells are commonly observed, indicating cell death, a number that markedly increases after *MTG1* silencing. Analysis of floating and attached cells showed a significant increase in Caspase 3 cleavage upon *MTG1* depletion (Supplementary Figure S2B and C). This phenotype was also observed in rho<sup>0</sup> cells silenced for *MTG1*, indicating that the severe cell death induced by depletion of *MTG1* is independent of mtDNA genome and hence of mitoribosomes (Supplementary Figure S2C). Therefore, *MTG1* may perform an extraribosomal role whose characterization is beyond the scope of this manuscript. Involvement of mitoribosome components and AFs in regulation of apoptosis has been previously documented. Recently, pro-apoptotic proteins death associated protein 3, Bcl-2-interacting mitochondrial ribosomal protein and p52 (programmed cell death protein 9) have been respectively identified as the mS29, mL41 and mL65 components of the mitoribosome. Contrary to *MTG1*, however, silencing of each of these proteins make cells resistant to apoptosis (reviewed in (4)). Similarly, mouse embryonic fibroblasts KO for the GTPase NOA1 (C4orf14 or *MTG3*), a mtSSU AF, were found to be resistant to staurosporine-induced apoptosis (37). As for *MTG1*, however, depletion of ERAL1, another mitochondrial GTPase that plays an important role in the assembly of the 28S mtSSU by acting as a chaperone for the 12S mt-

rRNA, leads to apoptosis in HeLa (19) and HEK293T cells (38) although cell death occurred before a mitochondrial protein synthesis defect was manifested (38). Also, depletion of the human mitoribosome recycling factor is lethal in HEK293T cells, where reactive oxygen species (ROS) overproduction preceded any measurable translational defect (39). The mechanisms connecting the mitoribosome to apoptosis regulation require therefore further investigations.

Here, we also observed that the *MTG1*-KO 1F5 cells undergo progressive adaptation and recovery of significant respiratory competence. This phenotypic suppression is not due to the acquisition of extragenic mutations in the *16S rRNA*, as reported in yeast (30), nor to intragenic mutations in the allele expressing the truncated *MTG1* protein, but to an increase in the steady-state levels of this protein (not shown). Therefore, we routinely assessed the *MTG1* steady-state levels in the culture prior to performing any experiments.

### **MTG1 is required for efficient mitochondrial translation and OXPHOS function in HEK293T cells**

Following the observation that *MTG1* co-sediments with the mitoribosome, we examined the mitochondrial translation capacity of *MTG1*-depleted cells by following the incorporation of [<sup>35</sup>S]-methionine into newly synthesized mitochondrial polypeptides in the presence of emetine to inhibit cytoplasmic protein synthesis. *De novo* mitochondrial protein synthesis rates were markedly decreased in *MTG1*-KO 1F5 and more deeply in *MTG1*-KO 1F5 siMTG1-treated cells (Figure 2D) thus demonstrating a role for *MTG1* in mitochondrial translation.

Consistent with their protein synthesis defect, *MTG1*-depleted HEK293T cells exhibited decreased steady-state levels of mtDNA-encoded OXPHOS components, especially NDUFB8 (a CI subunit), COX1 and COX2 (two CIV subunits), as analyzed by denaturing immunoblotting (Figure 2E). Blue native-PAGE analyses further disclosed a decrease in the accumulation of OXPHOS complexes I, III, IV and V, which contain mtDNA-encoded subunits, whereas the level of complex II, formed exclusively by nucleus-encoded subunits, was not affected (Figure 2F). The OXPHOS complex deficiency resulted in decreased endogenous cell respiration in *MTG1*-KO 1F5 cells to a residual level of 30% of control that was further decreased to 10% after *MTG1* gene-silencing for 5 days (Figure 2G). Under the same conditions, the residual activities of complex IV (cytochrome *c* oxidase, COX) were ~40% and 14% of control cell activities (Figure 2G). We conclude that in HEK293T cells, *MTG1* is necessary for mitochondrial protein synthesis and, consequently, for the biogenesis and function of mitochondrial OXPHOS complexes.

### **MTG1 is necessary for proper human cardiomyocyte activity and zebrafish cardiac development**

Mutations in both nDNA and mtDNA affecting mitochondrial protein expression machinery and their constituents, including mitoribosome components, lead to devastating human disorders often manifesting as mitochondrial cardiomyopathies or encephalo-cardiomyopathies (5,40). For

this reason, we decided to test the consequences of MTG1 depletion in cardiomyocyte physiology and heart development using two different models.

First, we used iPS cell-derived human cardiomyocytes (iCell cardiomyocytes) obtained from Cellular Dynamics (Madison, WI). After 4 days of full culture accommodation, transient *MTG1* silencing for 4 days resulted in MTG1 steady-state levels attenuated to 40% compared to siNT transfection groups (Figure 3A), and mitochondrial translation capacity decreased to 50% (Figure 3B). As a result, steady-state levels of mtDNA-encoded proteins (COX1 and COX2) were reduced. Depletion of MTG1 also affected steady-state levels of mtLSU proteins (uL14, uL16, bL27 and bL36), suggesting a mitoribosome biogenesis defect (Figure 3A). To examine the physiological effects of MTG1 depletion on cardiomyocyte functions, we measured intracellular  $\text{Ca}^{2+}$  transient ( $[\text{Ca}^{2+}]_i$ ) and  $\text{Ca}^{2+}$  decay in a single cell base by using an IonOptix iCCD camera as reported (41) to record spontaneous action potentials from individual cells using the whole-cell current clamp technique. After 4 days of *MTG1* silencing, the cardiomyocyte beating rate was significantly decreased (Figure 3C), and the  $\text{Ca}^{2+}$  clearance was substantially delayed (Figure 3D), indicating that MTG1 function is essential for maintaining optimal cardiomyocyte physiology.

Second, we tested the role of MTG1 in developing zebrafish. For this purpose, 1–2 cell stage zebrafish embryos were injected with zebrafish *Mtg1* (*zf-Mtg1*)-targeting or standard control (STD) Morpholino to induce transient KO-*Mtg1*. Available antibodies against zebrafish mitochondrial proteins are scarce, and our anti-human MTG1 did not cross-react with the fish homolog. We only found the anti-human COX1 antibody to cross-react with the fish protein and used it as a surrogate to follow potential mitochondrial protein synthesis defects derived from MTG1 depletion. The silencing efficiency was tested in this way after 48-h post-fertilization (hpf) when the average steady-state levels of COX1 were below 40% compared to control (Figure 3E). After 96 hpf when the embryos required a functional developed cardiovascular system for respiration, two different doses of *zf-mtg1* morphants had significantly lower heartbeats than those in each same dose of STD morphants (Figure 3F). Interestingly, whereas all STD morphants had a normal shape, most *zf-Mtg1* morphants in the higher dose (78.75%) and a few at the lower dose (8.4%) displayed apparent anatomical abnormalities such as a kinked body, edematous chest or a combination of both (Figure 3F). To better understand the hierarchy of pathophysiological events, we dissected the data from 79 morphants treated with 50 nM *zf-Mtg1* into four different groups based on their anatomical phenotypes. From the total, 36.25% of morphants displayed only edematous chest, 5% only kinked body and 37.5% exhibited both phenotypes (Figure 3F). Notably, 21.5% of morphants had apparently normal shape, but their heartbeats were already significantly lower than those in the same dose of STD or lower dose of *zf-Mtg1* morphants (Figure 3F), indicating that the cardiovascular lesion induced by MTG1 depletion is an early event in developing zebrafish.

We believe that the phenotypes described in these models are not influenced by the secondary function of MTG1

on cell survival, since even very low levels of the protein are sufficient to maintain viability in HEK293T cells. Our data support a role of MTG1 in the maintenance of cardiac physiology and cardiac development and present the gene as a candidate when screening for the molecular bases of dilated and hypertrophic cardiomyopathies associated with mitochondrial translation and OXPHOS defects.

### MTG1 is essential for the formation of functional mtLSU and monosomes

A function for MTG1 in preserving mitochondrial protein synthesis is conserved across the different models tested. Henceforth, for all mechanistic studies on the role of MTG1 at the molecular level, we have used the amenable HEK293T model cell lines. Data presented in Figure 1 supplies information about the interaction of MTG1 with mtLSU and a more transient interaction with the monosome.

To explore whether MTG1 depletion affects mitoribosome accumulation, we first tested the steady-state levels of mtLSU and mtSSU subunit markers (Figure 4A). Immunoblot analyses showed that several mtLSU proteins including uL11, uL14, and in particular the late-assembly proteins uL16, bL27 and bL36 were significantly reduced (Figure 4A). Incidentally, the *B. subtilis* counterparts of these subunits require the bacterial MTG1 homolog RbgA for their incorporation into late-assembly intermediates (28,42). Subsequently, we followed the formation of the mtLSU ribonucleoprotein particle in MTG1-depleted mitochondria by sucrose gradient sedimentation analysis of whole-cell extracts (WCE) prepared in the presence of magnesium. The most obvious effect of MTG1 depletion was the virtual absence of 55S monosomes (Figure 4B). Otherwise, the sedimentation pattern of the mtLSU and mtSSU protein markers within the individual subunits was not changed in *MTG1*-KO 1F5-siNT- and *MTG1*-KO 1F5-si*MTG1*-treated cells, except for bL36, which accumulated in the top light fractions (Figure 4B). These data suggest that while the 39S mtLSU particle can form near to completion when MTG1 is limiting, at least bL36 cannot be efficiently incorporated into the mtLSU assembly line. The residual MTG1 expressed in *MTG1*-KO 1F5-siNT- and *MTG1*-KO 1F5-si*MTG1*-treated mitochondria co-sedimented with the mtLSU but monosome formation with the mtSSU appears to be impaired, as mentioned earlier (Figure 4B). To better compare the accumulation of MTG1 and MRP markers in WT and MTG1-depleted extracts, we ran in parallel, in a single gel, samples from the relevant sucrose gradient fractions (Figure 4C). We confirmed that the levels of mtLSU proteins were increased in the F6-7 fractions where the mtLSU peaks, except bL36. Furthermore, we can better appreciate how the increasing depletion of MTG1 progressively impairs 55S monosome formation (Figure 4C). The same fractions from gradients presented in Figure 4B were used to analyze the rRNA distribution by Quantitative reverse transcription polymerase chain reaction (RT-qPCR). Levels of *16S rRNA* in the mtLSU fractions were similar in WT and MTG1-depleted cells, but the later had enhanced relative levels of *12S rRNA* in the mtSSU fractions (Figure 4D), probably reflecting the

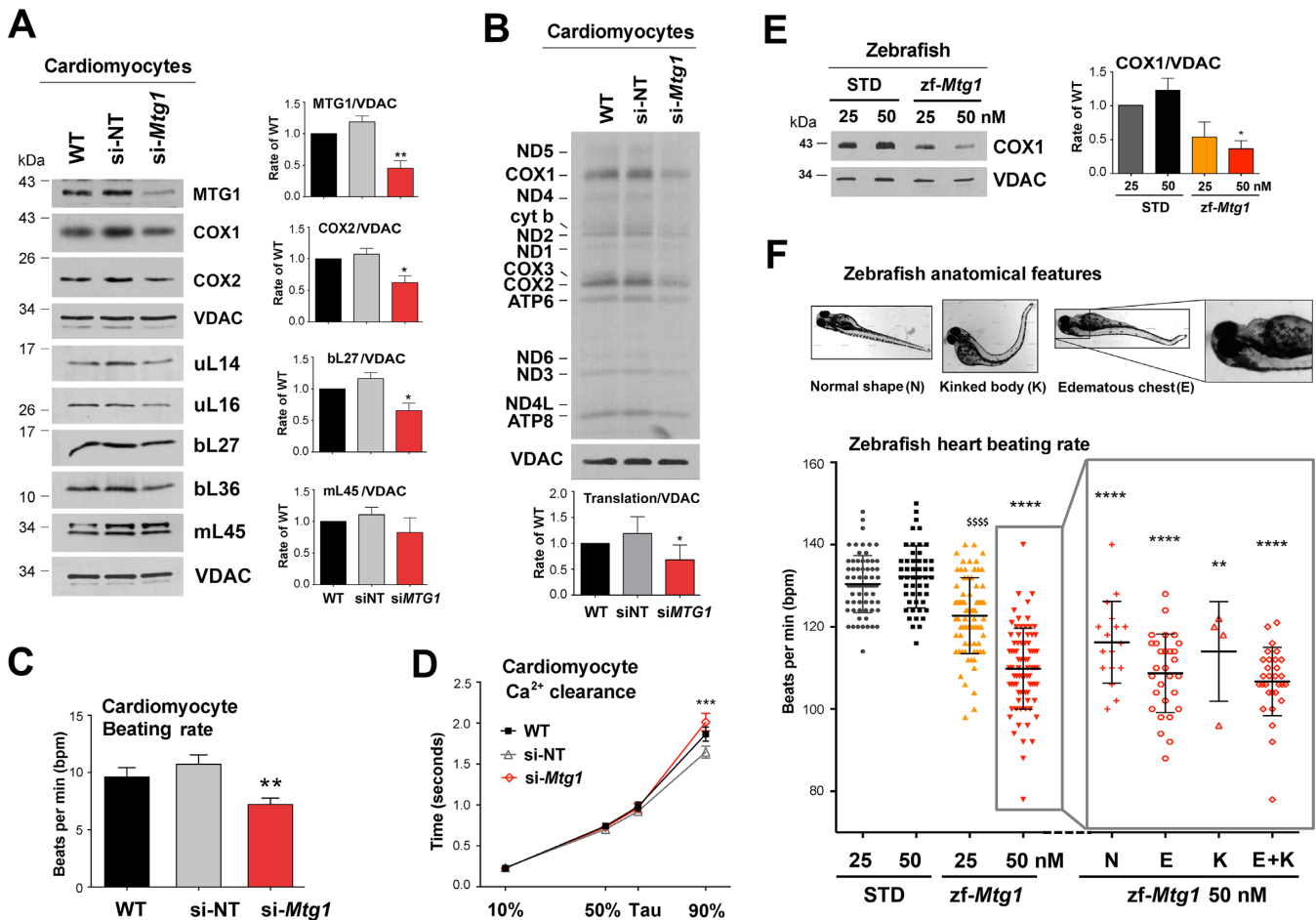


**Figure 3.** MTG1 is necessary for proper human cardiomyocyte physiology and zebrafish cardiac development. (A) Immunoblot analysis of the steady-state levels of MTG1, OXPHOS complex subunits and MRPs in iCell human cardiomyocytes left untreated (WT) or treated for 4 days with siNT or with siMTG1. VDAC was used as a loading control. The right panel shows the densitometry values normalized by the signal of VDAC and expressed relative to the WT. The bars represent average  $\pm$  SD.  $n = 4$ ; Student's two-tailed  $t$ -test: \* $P < 0.05$ ; \*\* $P < 0.01$ . (B) Metabolic labeling with <sup>35</sup>S-methionine of newly synthesized mitochondrial translation products in whole cells from the indicated lines during 30 min pulse in the presence of emetine to inhibit cytoplasmic protein synthesis. Immunoblotting for VDAC was used as a loading control. Newly synthesized polypeptides are identified on the right. The lower panel shows the densitometry values (average of all polypeptide signals) normalized by the signal of VDAC and expressed relative to the WT. The bars represent average  $\pm$  SD.  $n = 3$ ;  $t$ -test: \* $P < 0.05$ . (C) Cardiomyocyte beating rate. The bars represent average  $\pm$  SD.  $n = 4$ ; one-way ANOVA with Sidak's multiple comparisons test: \*\* $P < 0.01$ . (D) Cardiomyocyte physiology estimated by measuring Ca<sup>2+</sup> decay. Data represent the mean  $\pm$  SD of four independent repetitions. In each repetition, five cells from each group were analyzed; one-way ANOVA with a Sidak's multiple comparisons test: \*\*\* $P < 0.001$ . (E) Immunoblot analysis of the steady-state levels of COX1 as a mtDNA-encoded subunit marker in zebrafish embryos silenced for MTG1. The translation-blocking morpholino-targeting MTG1 exon 1 (zf-Mtg1, Gene Tools) and the standard scrambled morpholino (STD, Gene Tools) used as a control were injected at two different concentrations (25 or 50 nM) into 1–2 cell-stage embryos. At 48-h post-fertilization (hpf), 10 morphants from each group were pooled and used for immunoblotting. The graph on the right side shows the densitometry values of COX1 signal normalized by the signal of VDAC and expressed relative to the WT. Data represent the mean  $\pm$  SD of three independent repetitions; one-way ANOVA with a Tukey's multiple comparisons test: \* $P < 0.05$ . (F) Anatomical and cardiac features of zebrafish embryos injected with STD or zf-Mtg1. The upper panel presents representative images of zebrafish embryos at 96 hpf, depicting the several anatomical features observed. The lower panel graph presents the quantification of heart beating rates in the STD- or zf-Mtg1-treated groups. In each group, each symbol represents an individual embryo. On the right side of the graph, the zf-Mtg1 50 nM morphants were further divided into different groups based on their anatomical features. Data represent the mean  $\pm$  SD of four independent repetitions. Two-tailed  $t$ -test with a Mann–Whitney *post hoc* test. \* $P < 0.05$ , \*\* $P < 0.01$ , \*\*\* $P < 0.001$ , \*\*\*\* $P < 0.0001$ . N, normal shape; E, edematous chest; K, kinked body; E+K, a combination of kinked body and edematous chest.

lack of monosomes. In fact, quantification of total *12S* and *16 rRNAs* by northern blot and RT-qPCR did not identify any significant changes in their steady-state levels, which was also true for tRNA<sup>Val</sup> and several mRNAs analyzed (Figure 4E and F).

Finally, to obtain a more thorough picture of the differences in the composition and abundance of assembled mitoribosomal subunits, sucrose gradient fractions corresponding to the monosome, mtLSU and mtSSU

were methanol/chloroform precipitated and analyzed by mass spectrometry (Supplementary Figure S3). Consistent with the data presented in Figure 4B and C, all mtLSU and mtSSU proteins from MTG1-depleted mitochondria showed a decrease in the monosome fraction. Interestingly, the abundance of some proteins subunits tended to increase in the mtLSU fraction despite the reduced levels of some mtLSU proteins in total cell lysates (Supplementary Figure S3A), suggesting that those proteins able to integrate into



ribonucleoprotein particles could be more stable than when unassembled. bL36 was not detected, and bL35 was found particularly underrepresented.

These two proteins are among the late-assembly mtLSU proteins that accumulate in substoichiometric amounts in the 45S particle found in RbgA-depleted *B. subtilis* cells (22,28,29) and *Nicotiana benthamiana* chloroplasts (43). Because mutations in *B. subtilis* L6 attenuate the growth defect of an *rbgA* mutant (26), it has been proposed that RbgA may facilitate proper interaction between L6 and the maturing 50S ribosome, subsequently triggering the incorporation of the late-assembly proteins such as L16, L27, L28, L33a, L35 and L36. However, L6 is not present in the mitochondrial ribosome despite robust conservation of the rRNA to which it binds (see next section). This loss is structurally compensated by mitochondria-specific proteins mL66 (MRPS18a) and mL53 (44), which are not particularly under-represented in the mtLSU particles detected in the absence of human MTG1 (Figure 4A and Supplementary S3A). In yeast, the RbgA homolog Lsg1 has been proposed to play a role in the incorporation of the L16 homolog Rpl10 and other late-assembly proteins into the cytoplasmic LSU (45,46), suggesting that RbgA and its homologs regulate a step during LSU biogenesis that must be at least broadly conserved during evolution. In human cells, total mitochondrial bL16 levels are attenuated (Figure 4A), but they accumulated normally in the MTG1-less mtLSU particles (Figure 4C and Supplementary S3A).

Taken together, our data allow us to conclude that human MTG1 catalyzes a step that is required for the efficient incorporation of at least bL36 and bL35 during the late stages of mtLSU biogenesis.

### MTG1 catalyzes an mtLSU late-assembly step during the hierarchical incorporation of MRPs

We aimed to further examine the role of MTG1 during the hierarchical incorporation of MRPs and the ordered action of AFs during mtLSU biogenesis. For this purpose, we introduced siRNA-induced silencing of selected mtLSU proteins (Figure 5A) and AFs in WT cells and tested genetic interactions among them by immunoblotting (Figure 5B and C) and sucrose gradient sedimentation assays (Figure 5D).

The selected mtLSU proteins included early-assembled proteins such as bL19 and mL45 (6). As expected, silencing of bL19 or mL45 significantly lowered the steady-state levels of most mtLSU proteins, prevented mtLSU assembly and also attenuated MTG1 levels (Figure 5B and C), further confirming that MTG1 steady-state levels depend on mtLSU components. mL45 is the homolog of yeast Mba1, a ribosome membrane anchoring protein (47), whose incorporation at an early stage may serve to tether the 39S mtLSU at the inner membrane during subsequent steps in assembly. Hence, MTG1 acts beyond the incorporation of early assembly subunits.

We also included proteins that structurally compensate for the loss of L6, a proposed MTG1-functionally interacting protein, such as the mitochondria-specific protein mL66 (MRPS18a) (44), as well as for other structurally interconnected intermediate-binding proteins (uL14 and uL16) and AFs, such as C7orf30 also known as MALSU1. MALSU1

acts as a chaperone of uL14 (48,49), whose incorporation into the assembling 39S particle involves a conformational change of the sarcin-ricin loop (SRL, helix 95) in the 16S rRNA (50). The SRL is essential for assembly of the functional LSU core as well as for GTP-catalyzed steps of translation (51), specifically for anchoring elongation factor G (EF-G) on the ribosome during mRNA-tRNA translocation (52). The crystal structure of bacterial LSU revealed that SRL interacts with the body of the 50S LSU through the C-terminus domain of uL6 and loop-loop tertiary interactions with 23S rRNA h91. H91 then contacts h89, h90 and h92, which are connected directly to the A- and P-tRNA binding sites and the peptidyl transfer center (PTC). H91 also contacts h42, which connects to the GTPase-associated center (GAC; h43 and h44), indicating that SRL is linked with several critical regions of the 50S subunit by its tertiary interactions. In bacteria, uL6 is a two-domain protein. L6 N-terminus interacts with h97 of the 23S rRNA and its C-terminus interacts with the SRL. All mutations in L6 that suppress the mtLSU assembly defect in *rbgA*-deficient *B. subtilis* cluster in a region where the L6 closely contacts with 23S rRNA H97 (26). Also, the mutant L6 protein was stably incorporated into the 50S subunit, but markedly disrupted the formation of intact 70S ribosomes as a result of the improper positioning of the intersubunit bridge involving h89, which makes direct contact with L6 and uL16 (26). As explained earlier, uL6 is absent in mammalian mitochondria despite strong conservation of the uL6 binding rRNA helices, although the mitochondria-specific proteins mL66 and mL53 compensate for the loss of bacterial uL6 without functional replacement (44).

Based on the observations made in bacteria, we hypothesized a potential structural interaction among uL14, uL16, mL66, MALSU1 and MTG1 around the mtLSU functional core. Silencing of uL14 or MALSU1 affected their reciprocal stability and decreased the steady-state levels of uL16 (the effects of siMALSU1 were milder), indicating that uL16 incorporates after uL14 (Figure 5B and C). Also, the level of MTG1 was increased (Figure 5B and C) but at least the absence of uL14 prevented MTG1 binding to the mtLSU (Figure 5D), strongly indicating that MTG1 acts on the uL14-containing 39S pre-particle. We noticed an inverse correlation between the levels of MALSU1 and MTG1, which may reflect compensatory mechanisms or some functional interaction between these two GTPases through uL14. The level of uL16 was not particularly affected by MTG1 silencing. However, silencing of mL66, which structurally balances the absence of uL6, dramatically decreased the steady-state level of uL16, and significantly increased MALSU1 and MTG1 (Figure 5B and C). These data indicate that as for L6 in bacteria, mammalian mL66 is required for the proper incorporation of uL16 and other late-assembly proteins. Yet, mL66 silencing did not prevent incorporation of at least a small fraction of MTG1 into the mtLSU (Figure 5D). The decreased incorporation of MTG1 upon mL66 depletion indicates that MTG1 binding is enhanced or stabilized by the presence of mL66 and suggests that MTG1 might act to remodel the interaction of mL66 with the 16S rRNA after its incorporation into the mtLSU assembly line.

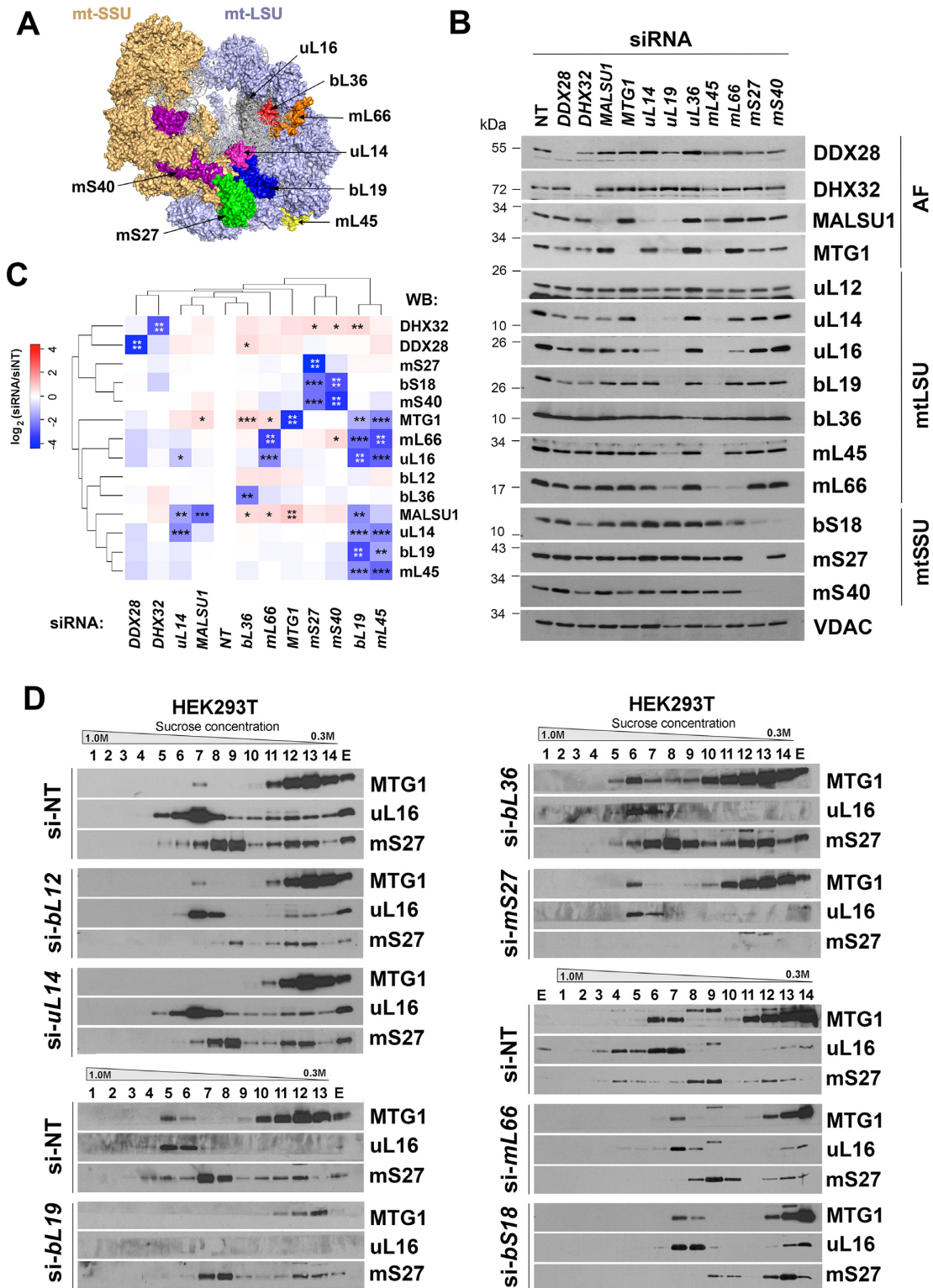


**Figure 5.** MTG1 catalyzes a mtLSU late-assembly step during the hierarchical incorporation of MRPs. Knockdown (KD) of mitoribosome AFs and mitoribosome subunits in HEK293T cells using siRNAs for 8–9 days, verified by immunoblotting of whole-cell lysates. (A) siRNA-targeted MRPs mapped to the human mitoribosome structure (PDB 3J9M) (2). (B) Representative image of immunoblot analysis of the steady-state levels of MRPs after silencing of target proteins. siRNA-NT is a non-targeting silencing control. Antibodies are listed on the right side, and VDAC was used as a loading control. (C) Following analysis in panel (B), the densitometric data obtained on the abundance of MRPs and AFs accumulated after silencing of each target protein were used for cluster analysis (see STAR Methods). The heat map, generated with the R studio software, represents a log<sub>2</sub> scale of the normalized average levels of ratio to control (NT) in three independent repetitions of immunoblotting analyses. VDAC was used as a loading control. Two-way ANOVA followed by a Dunnett’s multiple comparisons test: \**P* < 0.05; \*\**P* < 0.01; \*\*\**P* < 0.001). (D) Sucrose gradient sedimentation analysis of MTG1 and MRPs from mitochondrial extracts from the indicated cell lines. For each experiment, siNT-treated WT HEK293T cells were used as a control.

Our data exposed genetic interactions among the three S18 variants present in the mammalian mitoribosome (MRPS18a or mL66 in mtLSU, MRPS18b or mS40 and MRPS18c or bS18 in mtSSU), which were derived from gene duplication events from the same ancestral sequence (47). As expected, silencing of mL66 did not affect the levels of mS40 or bS18, and silencing of mS40 resulted in significantly decreased bS18 levels. mS40 silencing also enhanced mL66 levels, which could be a compensatory mechanism for the loss of mtSSU, since a similar (although not significant) tendency was observed in the absence of mS27 (Figure 5B and C). Silencing of mtSSU proteins did not affect the overall levels of mtLSU proteins or the interaction of MTG1 with the mtLSU (Figure 5D), thus supporting the notion that the mtLSU assembles independently of the mtSSU.

Finally, our study also incorporated silencing of mtLSU late-assembly protein bL36. In the mature mtLSU structure, bL36 was found only in a class of particles with folded *16S rRNA* at the intersubunit interface. This observation suggested that the recruitment of bL36 and the folding of mt-rRNA may be interdependent in a way that bL36 stabilizes tertiary interactions among h89, h91 and h97 (50). Because bacterial L6 has broad interactions with these helices, we asked how bL36 genetically interacted with other mtLSU proteins around the functional cores. Whereas depletion of bL36 did not significantly affect the levels of the mtLSU proteins analyzed, it leads to the marked accumulation of MTG1 as well as other mtLSU AFs, MALSU1 and the DEAD-box helicase DDX28 (Figure 5B and C). MTG1 co-sediments with the bL36-depleted mtLSU pre-particle (Figure 5D), which together with the observation that the steady-state levels of bL36 are remarkably decreased following depletion of MTG1 (Figures 4A–C and 5B), allowed us to conclude that bL36 is incorporated following the action of MTG1, similar to what has been described for bacterial RbgA (28,29).

Mass spectrometry analysis of the 55S monosome and 39S mtLSU from MTG1-depleted cells allowed us to further evaluate the hierarchy of incorporation of AFs during mtLSU assembly (Figure 5C and Supplementary S3B). Levels of the DEAD-box helicase DDX28 were maintained constant, suggesting early incorporation and stable interaction with the mtLSU particle assembled in the absence of MTG1 (Figure 5C and Supplementary S3B). On the contrary, levels of the GTPase MTG2 on the mtLSU were reduced following MTG1 depletion, indicating a labile interaction. Considering that yeast Mtg2 acts in steps before Mtg1 (9), it is conceivable that human MTG2 could be released from the growing particle before MTG1 incorporation.

### MTG1 directly interacts with the *16S ribosomal RNA*

The bacterial homolog of MTG1, RbgA, interacts with the LSU rRNA to promote a conformational change that permits incorporation of late-assembly LSU proteins (25). Thus, we set to examine whether MTG1 directly binds to the *16S rRNA* that could also allow us to propose the conformation rearrangement hypothesis. For this purpose, mitochondrial extracts from WT cells stably expressing MTG1-

FLAG were subjected or not to ultraviolet (UV)-mediated protein–nucleic acid cross-linking, anti-FLAG bead-driven IP as well as non-FLAG bead-driven IP as a control, and isolation of the co-immunoprecipitated (co-IPed) RNA. Following reverse transcription and qPCR analysis, the *12S rRNA* was poorly detected in all the different groups. In contrast, the *16S rRNA* was significantly enriched in the FLAG Co-IP eluted samples compared to those in the control IP. We amplified the *16S rRNA* using primers targeting three different regions of the gene (Figure 6A), and all three regions of *16S rRNAs* were highly enriched in MTG1 pulled-down eluates, thus demonstrating interaction of MTG1 with the *16S rRNA in vivo* (Figure 6B). Importantly, levels of detected *16S rRNA* were significantly lower in the UV-irradiated samples compared to those non-UV-irradiated, except those corresponding to the 3'-end of *16S rRNA* (Figure 6B). Since UV irradiation is known to induce RNA cleavage and degradation (53–55), we interpret these data as to indicate that MTG1 binds near the 3' end of the *16S rRNA* and protects that domain from UV-induced RNA cleavage. The *16S rRNA* 3'-end corresponds to domain VI, which includes helices 95–99 (Figure 6C).

As an alternative approach to identify and narrow the MTG1 target mitochondrial RNA transcripts, we isolated the co-IPed RNA, and performed pair-end RNA sequencing (RNA-seq) experiments (Figure 6D). This analysis clearly showed that MTG1 bound the *16S rRNA*, with major specificity for the region encompassing domain VI of the *16S rRNA* helices H95 (the SRL), H96 and H97. A schematic of the secondary structure of this domain indicating the helices with which mtLSU proteins interact is presented in Figure 6C.

Hence, our data show that MTG1 binds to a *16S rRNA* region conserved in bacteria that is remodeled following interaction with RbgA to facilitate incorporation of L35, L36 and other late-assembly proteins.

### MTG1 interacts with uL19 and mS27

In addition to interacting with rRNA, MTG1 could directly guide insertion of ribosomal proteins into the growing mtLSU particle. To identify potential mitoriboprotein interacting partners of MTG1, we used an array of approaches. Although we have detected a portion of total MTG1 co-sedimenting with the mtLSU, the interaction could be labile depending on GTP hydrolysis. To stabilize potential interactions, we performed immunoprecipitation (IP) assays with mitochondria incubated in the presence or absence of non-hydrolysable GTP (GMPPCP or  $\beta,\gamma$ -methylenguanosine 5'-triphosphate sodium salt) or chemical cross-linkers.

In one assay, mitochondria purified from HEK293T cells stably expressing FLAG-tagged MTG1 were pre-incubated with 2.5 mM GMPPCP for 40 min at 4°C to trap the transient MTG1–mitoribosome complex by blocking MTG1 dissociation. After lysis with mild 0.25% digitonin to maintain native complexes intact, the MTG1-FLAG-interacting proteins were isolated by FLAG-affinity IP and analyzed by immunoblotting. Whereas mtSSU proteins were not detected in the bound fractions, all mtLSU proteins analyzed were detected in the FLAG Co-IP eluate, but not in the

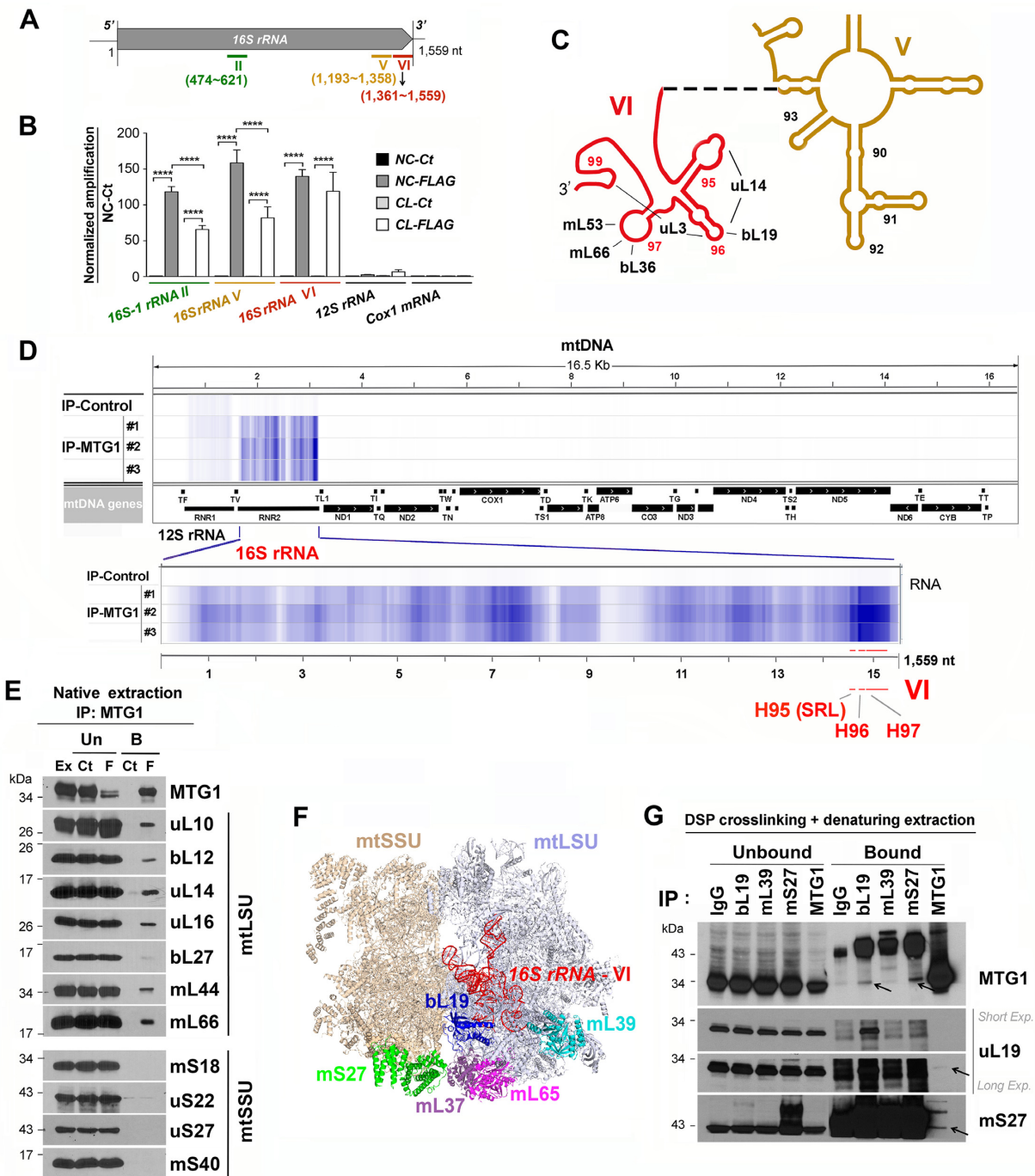


**Figure 6.** MTG1 directly binds to the mtLSU through the 16S ribosomal RNA and MRP uL19. (A) Scheme depicting the human 16S rRNA gene and the position of three different oligonucleotide pairs used for gene amplification of domains II, V or VI. (B) qPCR analyses of reverse-transcribed control (Ct) or MTG1-FLAG (FLAG) co-immunopurified RNAs after 4-thiouridine (4SU) treatment and non-crosslinked (NC) or UV-mediated protein–RNA cross-linking (CL). (C) 2D structure of 16S rRNA domains V and VI presenting helices, and VI-interacting LSU proteins indicated. (D) Identification of mtRNA targets of MTG1 by single-read-RNA-seq analysis of RNA isolated from IP experiments presented in panel (B). The graph represents a heat map of the normalized average density of the reads across the mitochondrial genome. Control sample represents non-specific binding of mitochondrial RNA to the naked beads (no antibody used for immunoprecipitation). Three independent repetitions are presented. Reads were pre-processed to remove sequencing adapters using Trimmomatic and then mapped with Tophat version 2.1.0 to the reference human genome (assembly GRCh37). Mitochondrial coverage was computed using Bedtools. Raw data can be accessed through the Gene Expression Omnibus (GEO) database repository (accession number GSE116688). (E) Co-IP analysis of MTG1-FLAG and native interacting MRPs with anti-FLAG agarose beads (F) or plain beads used as control (Ct). (F) Localization of the highly ranked MTG1 interacting mitoribosomal proteins (uL19, mS27, mL37, mL39 and mL65) and 16S rRNA domain VI (red) in the human mitoribosome structure (PDB 3J9M) (2). (G) IP analyses of endogenous bL19, mL39 or mS27 using Abs targeting each subunit from HEK293T cells stably expressing MTG1-FLAG. The interaction was fixed by incubation with the cleavable cross-linker DSP. IP with IgG was used as a negative control (IgG), and IP with anti-FLAG beads was used for pull-down of MTG1 as a positive control (MTG1). See also Supplementary Table S1. The statistical tests of MTG1–rRNAs interaction were analyzed with two-way ANOVA followed by a Tukey’s *post hoc* test (\*\*\*\**P* < 0.0001).

control-IP, demonstrating the native interaction of MTG1 with mtLSU proteins (Figure 6E). It is mechanistically relevant, however, that following pre-incubation with GMP-PCP we did observe only a mild increase in the portion of MTG1 that co-sediments with the mtLSU (Supplementary Figure S4), which suggests that the number of GTP-bound MTG1 molecules interacting with the mtLSU in our preparations is near saturation.

In another set of assays, we explored the interaction of MTG1 with mitoribosomal proteins in the presence of cross-linkers followed by extraction under denaturing conditions. First, we explored the directly interacting partners of MTG1 by using the cleavable cross-linker dithio-bis[succinimidylpropionate] (DSP). DSP has NHS-ester reactive ends that react toward amino groups, with a 12.0 Å spacer arm that contains a cleavable disulfide bond. Mitochondria were incubated in the presence DSP or the vehicle Dimethyl Sulfoxide (DMSO) as a negative control before extraction with 1% sodium dodecyl sulphate (SDS), dilution to final 0.1% SDS and FLAG affinity IP. In these conditions, MTG1 was IPed with several mtLSU markers tested, and also with some mtSSU proteins such as mS22, mS27 and mS40 (data not shown).

Subsequently, we used the non-cleavable cross-linker N- $\alpha$ -maleimidoacet-oxysuccinimide ester (AMAS). AMAS has NHS-ester and maleimide groups, which cross-link amino to sulfhydryl groups with a 4.4 Å spacer arm. Mitochondria purified from cells stably expressing MTG1-FLAG were incubated in the presence of AMAS or DMSO as a negative control, pulled-down with anti-FLAG agarose beads and analyzed by sodium dodecyl sulphate-polyacrylamide gel electrophoresis. After Coomassie staining, a band of ~75 kDa was observed only in the crosslinked-IPed sample (not shown). The band was cut, and its composition was analyzed by mass spectrometry. In two independent trials, we found that 13 MRPs were detected from each experiment, nine of which were overlapping (Supplementary Table S1). Given the MW of these proteins, MTG1 could be expected to interact with one of them, although it is conceivable that more than one MTG1 complex of similar MW could conform the ~75 kDa adduct. Also, some pairs of MRPs could be cross-linked and co-migrate with the MTG1-MRP adduct/s. While mapping these MRPs to the structure of the mitoribosome, we noticed that the five common MRPs with the higher rank, mS27, uL19, mL37, mL39 and mL65 locate adjacent to each other around the area where the mitochondria-specific bridge mB6 is formed by uL19 and mS27 (Figure 6F). Furthermore, these MTG1-interacting MRPs map to the location where the *16S rRNA* 3' end resides (Figure 6F).

Finally, to confirm the interaction of those MRPs with MTG1, we performed multiple reciprocal pull-down analyses using DSP-crosslinked mitochondrial extracts and anti-MRP-specific antibodies with protein A-sepharose beads. In these assays, we detected co-immunopurified fraction of MTG1 from elutes that incubated with a uL19 or mS27 antibody (Figure 6G). Beads conjugated to IgG or to mL39 were used as negative controls. Re-analyzing the mass spectrometry data of the AMAS-crosslinked adducts, we found that MTG1 co-immunopurified with uL19 and mS27 with over 95% of probability (Supplementary Table S2), con-

firmed that MTG1 directly interacts with uL19 and mS27. These results are in agreement with the observations made in sucrose gradient sedimentation analysis of WCE that detected a larger portion of MTG1 co-sedimented with the mtLSU but also a minor fraction co-sedimenting with the monosome (Figure 1).

During translation, multiple molecular contacts between the mature ribosomal subunits termed intersubunit bridges keep the monosome together and serve to control dynamics that enable the various steps of translation (56). Whereas in bacteria and eukaryotes, these bridges mainly involved conserved RNA-RNA interactions (57), the interface of the human mitoribosome is richer in protein-mediated connections (2,3). Several bridges present in bacterial ribosomes are absent in mitoribosomes, which in turn contain six mammalian mitochondrion-specific bridges, among them, bridge mB6 (also called B9) that is formed between uL19 and mS27 (2,3). Whereas the formation and function of mitoribosome intersubunit bridges remain to be understood, our observations allow us to propose a model in which MTG1 could directly or indirectly participate in either connecting or preventing the premature connection of uL19 and mS27.

In this model, MTG1 would bind to the *16S rRNA* to catalyze a late-stage mtLSU assembly step involving remodeling of the uL19-containing mtLSU domain. MTG1 would subsequently remain bound to the 39S mature particle and eventually released, hence facilitating the formation of the mB6 intersubunit bridge.

### MTG1 release from the 39S mtLSU is stimulated by mS27

GTPases work by cycling between inactive GDP-bound and active GTP-bound states. The interconversion of these states is facilitated by guanine nucleotide exchange factors (GEFs) and GTPase-activating proteins (GAPs). GEFs stimulate the release of GDP and then catalyze the GDP-GTP exchange, and GAPs accelerate GTP hydrolysis (58,59). Unlike prototypical GTPases, the characterized bacterial GTPases acting in ribosome assembly bind nucleotides weakly and are thus not expected to be dependent on GEFs to exchange GDP for GTP (60). Therefore, it has been proposed that most ribosome assembly GTPases could be directly regulated by the GTP/GDP ratio, which could allow these proteins to directly couple ribosome assembly to energy status in the cell (10,60). There is, however, at least one exception, *E. coli* RsgA, which catalyzes fast GTP hydrolysis in the presence of 50S LSU but then turnover is limited by GDP release, which is stimulated over 100-fold by the 30S ribosome acting as a GEF (61).

For the bacterial MTG1 homolog RbgA, GTP and GMPPNP were sufficient to promote RbgA association with a 45S intermediate, whereas only GMPPNP was able to support binding to the 50S subunit, likely due to the stimulation of GTP hydrolysis. Hence, RbgA has been proposed to promote a late step in ribosome biogenesis (discussed earlier), and one role of GTP hydrolysis is to stimulate its dissociation from the ribosome, which apparently does not need a GEF.

The case of MTG1 may be different. As for RbgA, a previous study reported that the intrinsic recombinant MTG1

GTPase activity is undetectable, but it is stimulated *in vitro* by the mtLSU and particularly by the 55S monosome (20). In human mitochondria, however, mS27 has been suggested to play a role as a GEF, as it shares sequence homology with the dibble-homology (DH) domain of the Dbl GEF family proteins (62). The DH domain interacts with the G protein and mediates the GEF activity. The alignment presented in Figure 7A shows weak but relevant primary sequence homology involving the C-terminus of mS27. The DH domain is constituted of three structurally conserved regions (CR1-3) separated by more variable regions (63). The three conserved regions, which are present in mS27 (Figure 7A), are known to contain some of the critical determinants of GEF function (63). Conserved residues include E185 and L197 in CR1, F235 in CR2 and LVKE (373–376) in CR3 (Figure 7A).

mS27 was initially thought to be a GEF for mS29 (64), a GTP-binding protein embedded in the SSU head, where it contributes to the formation of intersubunit bridges (2,3). However, the cryo-EM structures of the mammalian mitoribosome have located mS27 to the mtSSU foot, making impossible the mS29–mS27 functional association (2,3). Now, the physical interaction between MTG1 and mS27 described here (Figure 7B) opened the possibility for a functional relationship. We proposed that mS27 is a GEF of MTG1 that stimulates the release of GDP-bound MTG1 from uL19 in the mature mtLSU. To test this hypothesis, we used mitochondrial extracts from cells expressing FLAG-tagged MTG1 and performed IP assays to assess the amount of co-IPed uL19 when the extract was supplemented or not with recombinant mS27 (Figure 7B) obtained from Proteintech (Cat # Ag11223). The presence of excess GTP or GMPPCP did not affect the levels of co-IPed bL19, probably because the MTG1 molecules interacting with the mtLSU are already GTP bound. Importantly, however, incubation with excess recombinant mS27 significantly decreased the levels of co-IPed bL19 (Figure 7B). These data would be compatible with a scenario in which mS27 stimulates GDP–GTP interconversion in MTG1, promoting in this way the dissociation of GDP-bound MTG1 from the mature 39S mtLSU. Future studies on the *in vivo* role of mS27 as a GEF of MTG1 are warranted.

## CONCLUSION

Collectively, the data presented in this manuscript lead to a model for mitoribosome biogenesis in which MTG1 connects late-stage mtLSU assembly with mtSSU joining (Figure 8). In our model, MTG1 acts on mtLSU maturation in a manner broadly similar to its bacterial counterpart RbgA, with which it shares mechanistic principles (22,28,29), and also significant differences to attend to the specific mitoribosome composition and assembly pathway. MTG1 acts after MALSU1 whose binding to uL14 also induces conformational changes in the neighboring bL19 relative to their positions in the mature mitoribosome (50). Subsequently, GTP-bound MTG1 interacts with domain VI helices in the 16S rRNA and with protein bL19, presumably to induce a conformational change that facilitates incorporation of late-stage subunits, at least bL36 and bL35, to complete the mature 39S mtLSU particle. Then, MTG1 is not readily re-

leased from the mtLSU but remains bound to it, a behavior probably sustained by a slow MTG1 GDP–GTP exchange. The interaction of mtLSU/bL19-MTG1(GDP) with mS27 in the mtSSU promotes the previously unrecognized mS27 GEF activity on MTG1 that will facilitate GDP–GTP interchange and MTG1 release from the 55S monosome.

The proposed model has implications for translational regulation. We propose that MTG1 acts as an mtLSU quality control checkpoint molecule as it serves to avoid premature subunit joining. Redundant mechanisms exist to prevent premature subunit joining and translation initiation. An antisubunit-association activity has been also proposed for MALSU1, which belongs to the ribosome silencing factor (RsfS) family. MALSU1 forms a complex with two proteins, the mitochondrial acyl carrier protein and the LYR-motif-containing protein LOR8F8, which sterically obstructs the binding of the mtSSU (50). Also in bacteria, binding of RsfS to uL14 prevents the formation of bridge B8 with helix 14 of 16S rRNA (65). The subunit anti-association role of MTG1 is conserved for other members of its family, such as the *S. cerevisiae* protein Lsg1. In the cytoplasm, Lsg1 GTPase activity is required to release two 60S AFs, Nmd3, positioned across the PTC, and Tif6, from the 60S LSU (66) and allows 60S LSU interaction with 40S-initiation complexes (67).

Yeast and mammalian mitoribosomes have acquired an intrinsic GTPase in the small subunit, mS29 (68), an unique feature among ribosomes, which participates in subunit association. The identification of another mitochondrion-acquired mtSSU protein, mS27, absent in yeast, which acts as a GEF of MTG1 to catalyze the return of MTG1 from the inactive GDP-binding conformation to the active GTP-binding conformation, is also unprecedented in translational systems. Close examples include the protein elongation factor EF-Tu, which requires elongation factor EF-Ts for rapid exchange of GDP for GTP. In prokaryotes, free peptide release factor 3 is *in vivo* stably bound to GDP, and ribosomes in complex with RF1 or RF2 act as GEFs (69). The ribosome itself also acts as the GEF for EF-G that catalyzes the translocation of peptidyl-tRNA from the A site to the P site of the ribosome. The uniqueness of mS27 lies on the conservation of GEF motifs, its integration into the mitoribosome and its specificity for MTG1.

Finally, from a biomedical perspective, our genetic and physiological studies on HEK293T cells, human cardiomyocytes and zebrafish developing heart demonstrate the requirement of MTG1 for mitochondrial translation and OXPHOS function in multiple biological systems. Given the frequent clinical outcome of mitoribosome assembly and mitochondrial translation defects as pure or syndromic mitochondrial cardiomyopathies, our data highlight the deleterious potential of *MTG1* as a mitochondrial cardiomyopathy gene.

## DATA AVAILABILITY

Raw data can be accessed through the Gene Expression Omnibus (GEO) database repository (accession number GSE116688).

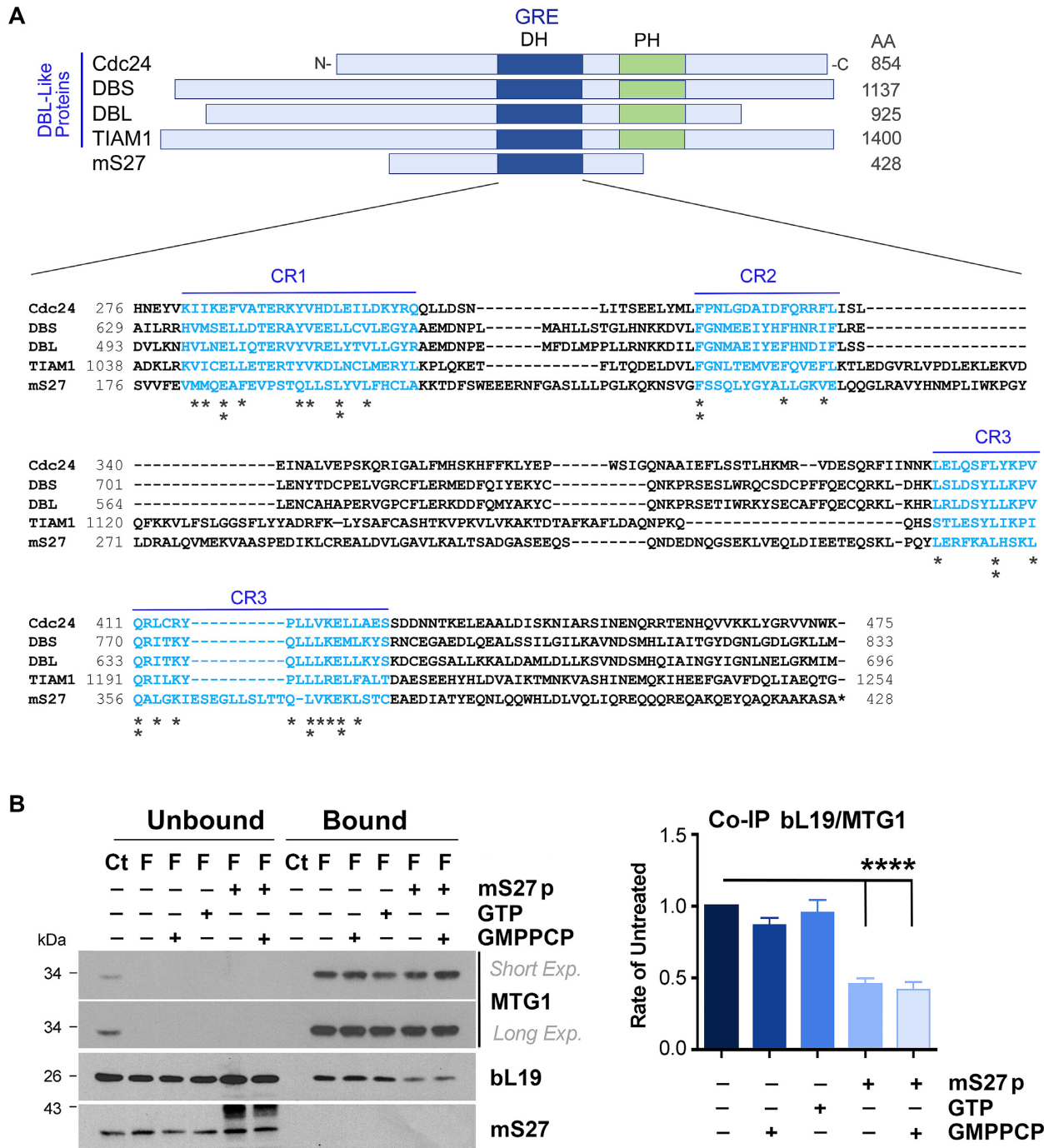


**Figure 7.** The mtSSU protein mS27 shares homology with Dbl GEF family proteins and promotes the release of MTG1 from the mitoribosome. (A) Schematics showing the structural domains present in several members of the Dbl GEF (GTP-exchange factor) family proteins (*Saccharomyces cerevisiae* Cdc24 and human DBS, DBL and TIAM1) in comparison with mS27. The catalytic region of most Rho-GTPase GEFs consists of a conserved DH/PH domain tandem (59). The DH domain, which interacts with the G protein and mediates the GEF activity, is conserved in mS27. The PH domain, commonly considered to be a phosphatidylinositol phosphate-binding protein domain structurally and functionally divergent in the individual GEFs, is absent in mS27. The lower panel shows a Clustal X alignment of human mS27 (NP.055899) with the Dbl GEF family proteins Cdc24 (DAA06945), DBL (P10911), DBS (O15068) and TIAM1 (NP.001340617). Conserved regions 1, 2 and 3 (CR1-3) are labeled in blue. A single asterisk indicates conserved residues and double asterisks identify identical residues. (B) Co-IP analysis of uL19 with MTG1-FLAG using anti-FLAG agarose beads, in the presence or absence of non-hydrolysable GTP (GMPPCP), hydrolysable GTP, recombinant mS27 (mS27p) or combination of GMPPCP with mS27. Ct, plain beads used as control; F, anti-FLAG agarose beads. The lower panel shows the densitometry values of co-immunopurified uL19 normalized by the signal of purified MTG1 and expressed relative to the untreated control. Data represent the mean  $\pm$  SD of five independent repetitions; one-way ANOVA with a Dunnett's multiple comparisons test, \*\*\*\* $P < 0.0001$ .

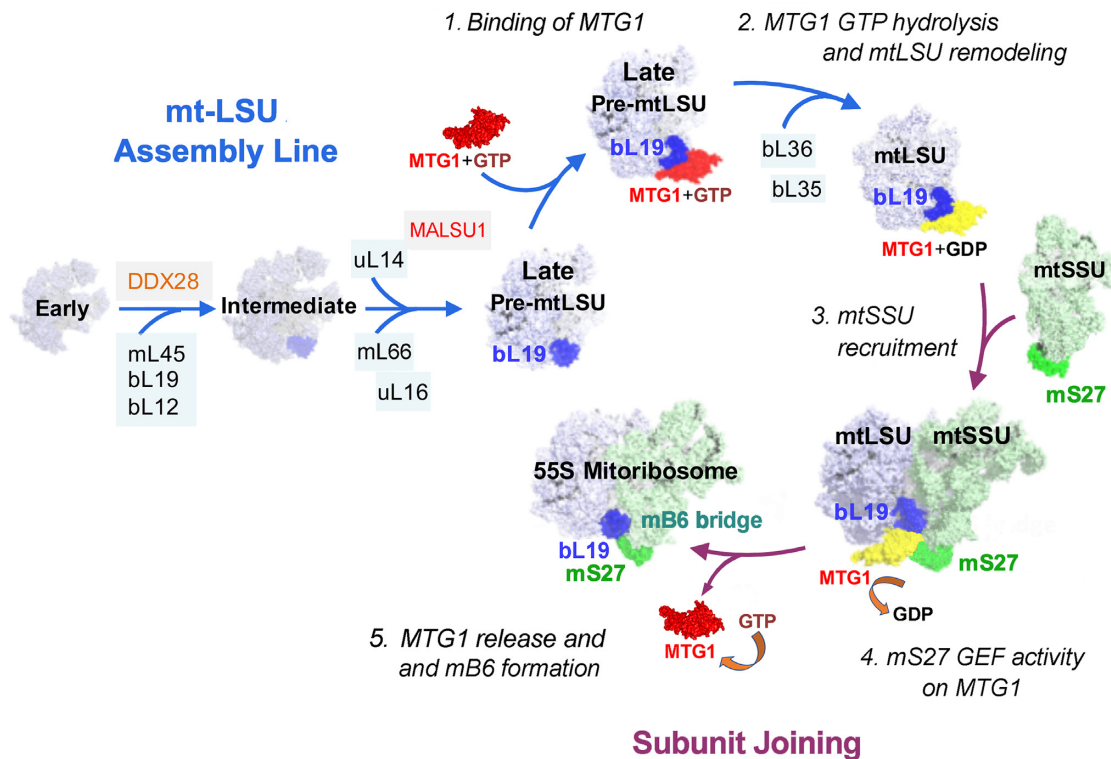


**Figure 8.** MTG1 is a GTPase that couples mtLSU assembly with intersubunit bridge formation. Model of 39S mtLSU biogenesis depicting the role of MTG1 in late steps of assembly and how these are connected to subsequent mtSSU subunit joining. The translation initiation complex is not represented for simplification. See explanation in the text.

## SUPPLEMENTARY DATA

Supplementary Data are available at NAR Online.

## ACKNOWLEDGEMENTS

We thank Dr Flavia Fontanesi, Dr Priyanka Maiti and Dr Alba Timon-Gomez for scientific discussions and comments on the manuscript. We thank Dr Brant Watson for proofreading. We thank Dr Raul A. Dulce and the Dr Joshua Hare lab for their technical assistance with the cardiomyocyte physiology studies.

*Author contributions:* H.J.K. generated the vast majority of the presented data. H.J.K. and A.B. designed the study, designed and performed experiments, analyzed results and wrote the paper.

## FUNDING

National Institutes of Health (NIH) Medical Sciences Maximizing Investigator's Award (NIGMS-MIRA) [R35GM118141 to A.B.]; Muscular Dystrophy Association Research Grant [MDA-381828 to A.B.]; American Heart Association Predoctoral Fellowship (to H.J.K.). Funding for open access charge: NIH [R35GM118141].

*Conflict of interest statement.* None declared.

## REFERENCES

- Margulis, L. (1975) Symbiotic theory of the origin of eukaryotic organelles; criteria for proof. *Symp. Soc. Exp. Biol.*, **29**, 21–38.
- Amunts, A., Brown, A., Toots, J., Scheres, S.H.W. and Ramakrishnan, V. (2015) The structure of the human mitochondrial ribosome. *Science*, **348**, 95–98.
- Greber, B.J., Bieri, P., Leibundgut, M., Leitner, A., Aebersold, R., Boehringer, D. and Ban, N. (2015) Ribosome. The complete structure of the 55S mammalian mitochondrial ribosome. *Science*, **348**, 303–308.
- Kim, H.J., Maiti, P. and Barrientos, A. (2017) Mitochondrial ribosomes in cancer. *Semin. Cancer Biol.*, **47**, 67–81.
- De Silva, D., Tu, Y.T., Amunts, A., Fontanesi, F. and Barrientos, A. (2015) Mitochondrial ribosome assembly in health and disease. *Cell Cycle*, **14**, 2226–2250.
- Bogenhagen, D.F., Ostermeyer-Fay, A.G., Haley, J.D. and Garcia-Diaz, M. (2018) Kinetics and mechanism of mammalian mitochondrial ribosome assembly. *Cell Rep.*, **22**, 1935–1944.
- Sashital, D.G., Greeman, C.A., Lyumkis, D., Potter, C.S., Carragher, B. and Williamson, J.R. (2014) A combined quantitative mass spectrometry and electron microscopy analysis of ribosomal 30S subunit assembly in *E. coli*. *Elife*, **3**, e04491.
- Woolford, J.L. Jr and Baserga, S.J. (2013) Ribosome biogenesis in the yeast *Saccharomyces cerevisiae*. *Genetics*, **195**, 643–681.
- Zeng, R., Smith, E. and Barrientos, A. (2018) Yeast mitoribosome large subunit assembly proceeds by hierarchical incorporation of protein clusters and modules on the inner membrane. *Cell Metab.*, **27**, 645–656.
- Britton, R.A. (2009) Role of GTPases in bacterial ribosome assembly. *Annu. Rev. Microbiol.*, **63**, 155–176.
- Wredenberg, A., Lagouge, M., Bratic, A., Metodiev, M.D., Spahr, H., Mourier, A., Freyer, C., Ruzzenente, B., Tain, L., Gronke, S. *et al.* (2013) MTERF3 regulates mitochondrial ribosome biogenesis in invertebrates and mammals. *PLoS Genet.*, **9**, e1003178.
- Camara, Y., Asin-Cayuela, J., Park, C.B., Metodiev, M.D., Shi, Y., Ruzzenente, B., Kukat, C., Habermann, B., Wibom, R., Hultenby, K. *et al.* (2011) MTERF4 regulates translation by targeting the methyltransferase NSUN4 to the mammalian mitochondrial ribosome. *Cell Metab.*, **13**, 527–539.

13. Metodiev, M.D., Spahr, H., Loguerio Polosa, P., Meharg, C., Becker, C., Altmueller, J., Habermann, B., Larsson, N.G. and Ruzzenente, B. (2014) NSUN4 is a dual function mitochondrial protein required for both methylation of 12S rRNA and coordination of mitoribosomal assembly. *PLoS Genet.*, **10**, e1004110.
14. Nolden, M., Ehses, S., Koppen, M., Bernacchia, A., Rugarli, E.I. and Langer, T. (2005) The m-AAA protease defective in hereditary spastic paraplegia controls ribosome assembly in mitochondria. *Cell*, **123**, 277–289.
15. Tu, Y.T. and Barrientos, A. (2015) The human mitochondrial DEAD-box protein DDX28 resides in RNA granules and functions in mitoribosome assembly. *Cell Rep.*, **10**, 854–864.
16. Strunk, B.S. and Karbstein, K. (2009) Powering through ribosome assembly. *RNA*, **15**, 2083–2104.
17. Karbstein, K. (2007) Role of GTPases in ribosome assembly. *Biopolymers*, **87**, 1–11.
18. He, J., Cooper, H.M., Reyes, A., Di Re, M., Kazak, L., Wood, S.R., Mao, C.C., Fearnley, I.M., Walker, J.E. and Holt, I.J. (2012) Human C4orf14 interacts with the mitochondrial nucleoid and is involved in the biogenesis of the small mitochondrial ribosomal subunit. *Nucleic Acids Res.*, **40**, 6097–6108.
19. Uchiumi, T., Ohgaki, K., Yagi, M., Aoki, Y., Sakai, A., Matsumoto, S. and Kang, D. (2010) ERAL1 is associated with mitochondrial ribosome and elimination of ERAL1 leads to mitochondrial dysfunction and growth retardation. *Nucleic Acids Res.*, **38**, 5554–5568.
20. Kotani, T., Akabane, S., Takeyasu, K., Ueda, T. and Takeuchi, N. (2013) Human G-proteins, ObgH1 and Mtg1, associate with the large mitochondrial ribosome subunit and are involved in translation and assembly of respiratory complexes. *Nucleic Acids Res.*, **41**, 3713–3722.
21. Goto, S., Muto, A. and Himeno, H. (2013) GTPases involved in bacterial ribosome maturation. *J. Biochem.*, **153**, 403–414.
22. Matsuo, Y., Morimoto, T., Kuwano, M., Loh, P.C., Oshima, T. and Ogasawara, N. (2006) The GTP-binding protein YlqF participates in the late step of 50 S ribosomal subunit assembly in *Bacillus subtilis*. *J. Biol. Chem.*, **281**, 8110–8117.
23. Matsuo, Y., Oshima, T., Loh, P.C., Morimoto, T. and Ogasawara, N. (2007) Isolation and characterization of a dominant negative mutant of *Bacillus subtilis* GTP-binding protein, YlqF, essential for biogenesis and maintenance of the 50 S ribosomal subunit. *J. Biol. Chem.*, **282**, 25270–25277.
24. Gulati, M., Jain, N., Anand, B., Prakash, B. and Britton, R.A. (2013) Mutational analysis of the ribosome assembly GTPase RbgA provides insight into ribosome interaction and ribosome-stimulated GTPase activation. *Nucleic Acids Res.*, **41**, 3217–3227.
25. Achila, D., Gulati, M., Jain, N. and Britton, R.A. (2012) Biochemical characterization of ribosome assembly GTPase RbgA in *Bacillus subtilis*. *J. Biol. Chem.*, **287**, 8417–8423.
26. Gulati, M., Jain, N., Davis, J.H., Williamson, J.R. and Britton, R.A. (2014) Functional interaction between ribosomal protein L6 and RbgA during ribosome assembly. *PLoS Genet.*, **10**, e1004694.
27. Kim do, J., Jang, J.Y., Yoon, H.J. and Suh, S.W. (2008) Crystal structure of YlqF, a circularly permuted GTPase: implications for its GTPase activation in 50 S ribosomal subunit assembly. *Proteins*, **72**, 1363–1370.
28. Jomaa, A., Jain, N., Davis, J.H., Williamson, J.R., Britton, R.A. and Ortega, J. (2014) Functional domains of the 50S subunit mature late in the assembly process. *Nucleic Acids Res.*, **42**, 3419–3435.
29. Uicker, W.C., Schaefer, I. and Britton, R.A. (2006) The essential GTPase RbgA (YlqF) is required for 50S ribosome assembly in *Bacillus subtilis*. *Mol. Microbiol.*, **59**, 528–540.
30. Barrientos, A., Korr, D., Barwell, K.J., Sjulsen, C., Gajewski, C.D., Manfredi, G., Ackerman, S. and Tzagoloff, A. (2003) *MTG1* codes for a conserved protein required for mitochondrial translation. *Mol. Biol. Cell*, **14**, 2292–2302.
31. King, M.P. and Attadi, G. (1996) Mitochondria-mediated transformation of human rho (0) cells. *Methods Enzymol.*, **264**, 304–313.
32. Agostino, A., Invernizzi, F., Tiveron, C., Fagioliari, G., Prella, A., Lamantea, E., Giavazzi, A., Battaglia, G., Tatangelo, L., Tiranti, V. et al. (2003) Constitutive knockout of Surfl is associated with high embryonic lethality, mitochondrial disease and cytochrome c oxidase deficiency in mice. *Hum. Mol. Genet.*, **12**, 399–413.
33. Leary, S.C. and Sasarman, F. (2009) Oxidative phosphorylation: synthesis of mitochondrially encoded proteins and assembly of individual structural subunits into functional holoenzyme complexes. *Methods Mol. Biol.*, **554**, 143–162.
34. Bourens, M. and Barrientos, A. (2017) A CMC1-Knockout reveals translation-independent control of human mitochondrial Complex IV biogenesis. *EMBO Rep.*, **18**, 477–494.
35. Enriquez, J.A. and Attardi, G. (1996) Analysis of aminoacylation of human mitochondrial tRNAs. *Methods Enzymol.*, **264**, 183–196.
36. Hafner, M., Landthaler, M., Burger, L., Khorshid, M., Hausser, J., Berninger, P., Rothballer, A., Ascano, M. Jr, Jungkamp, A.C., Munschauer, M. et al. (2010) Transcriptome-wide identification of RNA-binding protein and microRNA target sites by PAR-CLIP. *Cell*, **141**, 129–141.
37. Kolanczyk, M., Pech, M., Zemojtel, T., Yamamoto, H., Mikula, I., Calvaruso, M.A., van den Brand, M., Richter, R., Fischer, B., Ritz, A. et al. (2011) NOA1 is an essential GTPase required for mitochondrial protein synthesis. *Mol. Biol. Cell*, **22**, 1–11.
38. Dennerlein, S., Rozanska, A., Wydro, M., Chrzanoska-Lightowlers, Z.M. and Lightowlers, R.N. (2010) Human ERAL1 is a mitochondrial RNA chaperone involved in the assembly of the 28S small mitochondrial ribosomal subunit. *Biochem. J.*, **430**, 551–558.
39. Rorbach, J., Richter, R., Wessels, H.J., Wydro, M., Pekalski, M., Farhoud, M., Kuhl, I., Gaisne, M., Bonnefoy, N., Smeitink, J.A. et al. (2008) The human mitochondrial ribosome recycling factor is essential for cell viability. *Nucleic Acids Res.*, **36**, 5787–5799.
40. Vafai, S.B. and Mootha, V.K. (2012) Mitochondrial disorders as windows into an ancient organelle. *Nature*, **491**, 374–383.
41. Dulce, R.A., Yiginer, O., Gonzalez, D.R., Goss, G., Feng, N., Zheng, M. and Hare, J.M. (2013) Hydralazine and organic nitrates restore impaired excitation-contraction coupling by reducing calcium leak associated with nitroso-redox imbalance. *J. Biol. Chem.*, **288**, 6522–6533.
42. Schaefer, L., Uicker, W.C., Wicker-Planquart, C., Foucher, A.E., Jault, J.M. and Britton, R.A. (2006) Multiple GTPases participate in the assembly of the large ribosomal subunit in *Bacillus subtilis*. *J. Bacteriol.*, **188**, 8252–8258.
43. Jeon, Y., Ahn, H.K., Kang, Y.W. and Pai, H.S. (2017) Functional characterization of chloroplast-targeted RbgA GTPase in higher plants. *Plant Mol. Biol.*, **95**, 463–479.
44. Brown, A., Amunts, A., Bai, X.C., Sugimoto, Y., Edwards, P.C., Murshudov, G., Scheres, S.H. and Ramakrishnan, V. (2014) Structure of the large ribosomal subunit from human mitochondria. *Science*, **46**, 718–722.
45. Hedges, J., West, M. and Johnson, A.W. (2005) Release of the export adapter, Nmd3p, from the 60S ribosomal subunit requires Rpl10p and the cytoplasmic GTPase Lsg1p. *EMBO J.*, **24**, 567–579.
46. West, M., Hedges, J.B., Chen, A. and Johnson, A.W. (2005) Defining the order in which Nmd3p and Rpl10p load onto nascent 60S ribosomal subunits. *Mol. Cell Biol.*, **25**, 3802–3813.
47. Smits, P., Smeitink, J.A., van den Heuvel, L.P., Huynen, M.A. and Ettema, T.J. (2007) Reconstructing the evolution of the mitochondrial ribosomal proteome. *Nucleic Acids Res.*, **35**, 4686–4703.
48. Fung, S., Nishimura, T., Sasarman, F. and Shoubridge, E.A. (2013) The conserved interaction of C7orf30 with MRPL14 promotes biogenesis of the mitochondrial large ribosomal subunit and mitochondrial translation. *Mol. Biol. Cell*, **24**, 184–193.
49. Rorbach, J., Gammage, P.A. and Minczuk, M. (2012) C7orf30 is necessary for biogenesis of the large subunit of the mitochondrial ribosome. *Nucleic Acids Res.*, **40**, 4097–4109.
50. Brown, A., Rathore, S., Kimanius, D., Aibara, S., Bai, X.C., Rorbach, J., Amunts, A. and Ramakrishnan, V. (2017) Structures of the human mitochondrial ribosome in native states of assembly. *Nat. Struct. Mol. Biol.*, **24**, 866–869.
51. Lancaster, L., Lambert, N.J., Maklan, E.J., Horan, L.H. and Noller, H.F. (2008) The sarcin-ricin loop of 23S rRNA is essential for assembly of the functional core of the 50S ribosomal subunit. *RNA*, **14**, 1999–2012.
52. Shi, X., Khade, P.K., Sanbonmatsu, K.Y. and Joseph, S. (2012) Functional role of the sarcin-ricin loop of the 23S rRNA in the elongation cycle of protein synthesis. *J. Mol. Biol.*, **419**, 125–138.
53. Ariza-Mateos, A., Prieto-Vega, S., Diaz-Toledano, R., Birk, A., Szeto, H., Mena, I., Berzal-Herranz, A. and Gomez, J. (2012) RNA

- self-cleavage activated by ultraviolet light-induced oxidation. *Nucleic Acids Res.*, **40**, 1748–1766.
54. Simonet, J. and Gantzer, C. (2006) Inactivation of poliovirus 1 and F-specific RNA phages and degradation of their genomes by UV irradiation at 254 nanometers. *Appl. Environ. Microbiol.*, **72**, 7671–7677.
  55. Fimognari, C. (2015) Role of oxidative RNA damage in chronic-degenerative diseases. *Oxid. Med. Cell. Longev.*, **2015**, 358713.
  56. Liu, Q. and Fredrick, K. (2016) Intersubunit bridges of the bacterial ribosome. *J. Mol. Biol.*, **428**, 2146–2164.
  57. Lilleorg, S., Reier, K., Remme, J. and Liiv, A. (2017) The intersubunit bridge B1b of the bacterial ribosome facilitates initiation of protein synthesis and maintenance of translational fidelity. *J. Mol. Biol.*, **429**, 1067–1080.
  58. Vetter, I.R. and Wittinghofer, A. (2001) The guanine nucleotide-binding switch in three dimensions. *Science*, **294**, 1299–1304.
  59. Kaser, M., Kambacheld, M., Kisters-Woike, B. and Langer, T. (2003) Oma1, a novel membrane-bound metallopeptidase in mitochondria with activities overlapping with the m-AAA protease. *J. Biol. Chem.*, **278**, 46414–46423.
  60. Daigle, D.M. and Brown, E.D. (2004) Studies of the interaction of *Escherichia coli* YjeQ with the ribosome in vitro. *J. Bacteriol.*, **186**, 1381–1387.
  61. Cavdar Koc, E., Burkhart, W., Blackburn, K., Moseley, A. and Spremulli, L.L. (2001) The small subunit of the mammalian mitochondrial ribosome. Identification of the full complement of ribosomal proteins present. *J. Biol. Chem.*, **276**, 19363–19374.
  62. Whitehead, I.P., Campbell, S., Rossman, K.L. and Der, C.J. (1997) Dbl family proteins. *Biochim. Biophys. Acta*, **1332**, F1–F23.
  63. Cavdar Koc, E., Ranasinghe, A., Burkhart, W., Blackburn, K., Koc, H., Moseley, A. and Spremulli, L.L. (2001) A new face on apoptosis: death-associated protein 3 and PDCD9 are mitochondrial ribosomal proteins. *FEBS Lett.*, **492**, 166–170.
  64. Li, X., Sun, Q., Jiang, C., Yang, K., Hung, L.W., Zhang, J. and Sacchettini, J.C. (2015) Structure of ribosomal silencing factor bound to *Mycobacterium tuberculosis* ribosome. *Structure*, **23**, 1858–1865.
  65. Ho, J.H. and Johnson, A.W. (1999) NMD3 encodes an essential cytoplasmic protein required for stable 60S ribosomal subunits in *Saccharomyces cerevisiae*. *Mol. Cell. Biol.*, **19**, 2389–2399.
  66. Malyutin, A.G., Musalgaonkar, S., Patchett, S., Frank, J. and Johnson, A.W. (2017) Nmd3 is a structural mimic of eIF5A, and activates the cpGTPase Lsg1 during 60S ribosome biogenesis. *EMBO J.*, **36**, 854–868.
  67. Denslow, N.D., Anders, J.C. and O'Brien, T.W. (1991) Bovine mitochondrial ribosomes possess a high affinity binding site for guanine nucleotides. *J. Biol. Chem.*, **266**, 9586–9590.
  68. Zavialov, A.V., Buckingham, R.H. and Ehrenberg, M. (2001) A posttermination ribosomal complex is the guanine nucleotide exchange factor for peptide release factor RF3. *Cell*, **107**, 115–124.
  69. Bos, J.L., Rehmann, H. and Wittinghofer, A. (2007) GEFs and GAPs: critical elements in the control of small G proteins. *Cell*, **129**, 865–877.